Shear Strengthening of Reinforced Concrete Walls with Externally Bonded FRP Fabrics

Jesús David Ortiz Polanco

Escuela Colombiana de Ingeniería Julio Garavito

Master's Degree in Civil Engineering

Bogotá D.C., Colombia

2020

Shear Strengthening of Reinforced Concrete Walls with Externally Bonded FRP Fabrics

Jesús David Ortiz Polanco

A thesis submitted in partial fulfillment of the requirements for the degree of master's in civil engineering with emphasis on Structural Engineering

Advisor:

Nancy Torres Castellanos, PhD.

Co-advisor:

Francisco J. De Caso y Basalo, PhD.

Line of Research:

Structural Behavior

Investigation Group:

GIMECI

Escuela Colombiana de Ingeniería Julio Garavito

Master's degree in civil engineering

Bogotá D.C., Colombia

2020

To my family

Master's Thesis entitled "Shear Strengthening of Reinforced Concrete Walls with Externally Bonded FRP Fabrics", submitted by Jesús David Ortiz Polanco, fulfill the requirements established to qualify for the master's degree in Civil Engineering with emphasis on Structural Engineering.

Advisor:

Nancy Torres Castellanos, M.Sc., PhD.

Co-advisor:

Francisco J. De Caso y Basalo, M.Sc., PhD.

Approved:

_____

Carlos Eugenio Palomino Arias, M.Sc., P.E.

Jury 1

_____

Luis Enrique Aycardi Fonseca, M.Sc.

Jury 2

Bogotá D.C., February 4th, 2021 (Approval date)

Acknowledgments

To my family and friends for their continuous motivation, who always believed in me and encourage me to keep pursuing my dreams and goals.

To Escuela Colombiana de Ingeniería for the support, to all structural and materials laboratory's staff, Cristian Cogollo, María Isabel Espejo, Luis Beltran, Ramón Torres and Jairo Páez who were always willing to help and support.

To the Dr. Francisco José de Caso y Basalo who believed in my capacities and was always willing to share his knowledge with me.

To the Dr. Sandra Jerez who was a fundamental part during the tests.

And especially to the Dr. Nancy Torres Castellanos for giving me the opportunity to be involved in different projects within the laboratory and who encouraged me since the first day to continue my personal and professional training, providing me with the tools and support to successfully develop this investigation. I want to thank you for your support and trust in my work.

Abstract

During recent seismic events, it has become evident that thin reinforced concrete walls (TRCW) can present failures due to the lack of confinement and boundary elements because of their thickness, which only allows a reinforcing steel grid. These failures are characterized by out-of-plane instabilities, flexural failures and shear failures. The last ones, brittle and sudden failures that could seriously compromise the stability of the structure. FRP reinforcements have shown in research around the world to have a great performance in different structural elements under different loads.

This document presents the results of a research project in which the behavior of the shear strengthening of thin reinforced concrete walls using different external FRP fabrics schemes and systems was evaluated, analyzing 10 specimens; 5 low concrete strength resistance and 5 high resistance, with dimensions of 0.1 x 1.3 x 2.6 m (4 x 52 x 102 in) with shear reinforcement deficiency reinforced with 2 carbon fibers (CFRP) and 1 glass fiber (GFRP).

The failure mode, the hysteretic response, the stiffness degradation, and the energy dissipation capacity were evaluated, showing significant improvements in the shear capacity for each specimen evaluated as well as differences in terms of the equations taken as a basis provided by the ACI 440.2 R - 17 for the calculation of the external reinforcement contribution and the experimental load capacity of each specimen.

Keywords: External Reinforcement, Thin Concrete Walls, FRP Fabrics, GFRP, CFRP.

Resumen

Durante eventos sísmicos recientes se ha evidenciado que los muros esbeltos de concreto reforzado pueden presentar fallas debido a la falta de confinamiento y elementos de borde producto de su espesor, que únicamente permite una parrilla de acero de refuerzo. Estas fallas están caracterizadas por inestabilidades fuera del plano, fallas por flexión y fallas por corte. Estas últimas, fallas súbitas y frágiles, podrían comprometer seriamente la estabilidad de la estructura. Los reforzamientos externos con bandas de polímeros reforzados con fibra (FRP) han demostrado en investigaciones alrededor del mundo tener un gran desempeño en diferentes elementos estructurales ante diferentes solicitaciones.

En el presente documento se exponen los resultados de un proyecto de investigación en donde se evaluó el comportamiento de diferentes esquemas y sistemas de FRP como material de refuerzo a corte en muros esbeltos de concreto reforzado, analizando 10 muros; 5 con concreto de baja resistencia a la compresión y 5 de alta resistencia, de 0.1 x 1.3 x 2.6 m (4 x 52 x 102 in) con deficiencia de refuerzo cortante; reforzados externamente con 2 tipos de fibras de carbono (CFRP) y 1 tipo de fibra de vidrio (GFRP).

Dentro del análisis se evaluó el modo de falla, la respuesta histerética, la degradación de rigidez y la capacidad de disipación de energía, mostrando mejoras significativas en la capacidad a cortante para cada uno de los reforzamientos externos considerados. De igual manera se encontraron diferencias en cuanto a las ecuaciones tomadas como base brindadas por el ACI 440.2R – 17 para el cálculo teórico del aporte del refuerzo y las capacidades experimentales.

Palabras clave: Reforzamiento externo, Muro esbelto de concreto, bandas de FRP, GFRP, CFRP.

Table of contents

Page.

List of Figures

Page.

List of Tables

Page.

.

List of Symbols and Abbreviations

The list of symbols and abbreviations that will be used throughout the document is presented below.

Symbols with Latin letters

Symbol	Term	SI Units	United States S. of Units
A_{fv}	Area of FRP external reinforcement	mm^2	in^2
d'	Reinforcement covering	m	in
d_w	Effective depth of the shear wall	m	in
E_f	Tensile modulus of elasticity of FRP	GPa	ksi
E_y	Tensile modulus of elasticity of steel	GPa	ksi
f'_c	Concrete strength	MPa	psi
f_{yl}	Yield strength of longitudinal reinforcement	MPa	psi
f_{yt}	Yield strength of transverse reinforcement	MPa	psi
h_w	Wall height	m	in
k_1	Modification factor that account for the concrete strength	-	-
k_2	Modification factor that account for the type of wrapping scheme used	-	-
L_e	Active bond length	m	in
l_w	Wall length	m	in
M_H	Moment produced by P_H	kN.m	kip.ft
M_L	Moment produced by P_L	kN.m	kip.ft
n	Number of plies of FRP reinforcement	-	-
P_H	Maximum point load for shear failure in high concrete strength TRCW	kN	kip
P_L	Maximum point load for shear failure in low concrete strength TRCW	kN	kip
$P_{n,FRP}$	Theoretical capacity strengthened specimen	kN	kip
$P_{nc,u}$	Theoretical capacity unreinforced specimen	kN	kip
$P_{u,exp}$	Experimental capacity of the specimen	kN	kip
S_f	Center-to-center spacing of FRP	m	in
t_f	Nominal thickness of one ply of FRP reinforcement	m	in
t_w	Wall thickness	m	in
V_f	Shear strength provided by the FRP	kN	kip
V_n	Nominal shear resistance of the wall by ACI 318-19	kN	kip
V_R	Theoretical shear strength of the wall	kN	kip
V_{RE}	Experimental shear strength of the wall	kN	kip

w_f	Width of FRP reinforcing plies	m	in

Symbols with Greek letters

Symbols	Term	SI Units	United States S. of Units
α_c		-	-
ΔP_{nFRP}	Contribution of the FRP the shear capacity of the wall	kN	kip
ε_{cu}	Maximum concrete strain	mm/mm	in/in
ε_{fe}	Effective strain in FRP reinforcement attained at failure	mm/mm	in/in
ε_{fu}	Design rupture strain of FRP reinforcement	mm/mm	in/in
ε_y	Yield steel strain	mm/mm	in/in
κ_v	Bond-reduction coefficient for shear	-	-
λ			
μ_u	Maximum deflexion recorded at last cycle of force control protocol	mm	in
ρ_l	Ratio of longitudinal steel reinforcement	-	-
ρ_t	Ratio of transverse steel reinforcement	-	-

Abbreviations

Abbreviation	Term
ACI	American Concrete Institute
AIS	Asociación Colombiana de Ingeniería Sísmica
CFRP	Carbon Fiber Reinforced Polymer
FRP	Fiber-Reinforced Polymer
GFRP	Glass Fiber Reinforced Polymer
LVDT	Linear Variable Differential Transformer
RCW	Reinforced Concrete Wall
SFRC	Steel Fiber Reinforced Concrete
TRCW	Thin Reinforced Concrete Wall

Introduction

Reinforced concrete walls are one of the most used earthquake resistance systems due to their industrialization (shorter construction times) and economy (lower costs than other structural systems, for example, moment-resisting frames). However, Laboratory tests around the world and earthquakes in countries such as Chile (2010) and New Zealand (2011) have shown that buildings constructed with relatively thin and slender reinforced concrete walls could result in significant damage to heritage and losses of human life. (CEER (Colombian Earthquake Engineering Research Network), 2018).

The industrialized system of thin reinforced concrete walls (TRCW) has demonstrated good resistant earthquake performance in low-rise buildings of up to 3 floors (Carrillo & Alcocer, 2012, 2013). This structural system is mainly used in medium and low social strata in consequence of its low prices, growing significantly despite having limited knowledge about its behavior in a seismic event and few experimental results in laboratory tests. Experimental observations on the seismic performance of thin walls and buildings affected by recent earthquakes such as Maule in Chile 2010 and Christchurch in New Zealand 2011 show that the behavior of slender walls may not be adequate under the action of seismic loads.

Investigations carried out by Oesterle (1976), Goodsir (1985), Thomsen and Wallace (2004), the CEER (CEER (Colombian Earthquake Engineering Research Network), 2018), San

Bartlomé (A. San Bartolomé et al., 2007) have found similar failures modes characterized for compression at the base and diagonal cracking.

As a consequence of the problematic above, it was intended to develop a reinforcement solution that aims to optimize the behavior of vulnerable buildings. This report seeks to assess the shear behavior of TRCW externally reinforced with fiber-reinforced polymer (FRP) fabrics when they are subject to cyclical lateral loads in the plane.

A series of tests on TRCW were proposed, starting from a wall design with deficient shear reinforcement to force shear failure and propose different alternatives of external reinforcement with fiber-reinforced polymer fabrics (FRP) based on ACI 440.2R – 17, Guide for the Design and Construction of Externally Bonded FRP Systems for Strengthening Concrete Structures (*American Concrete Institute (ACI) Committee 440. 440.2R-17: Guide for the Design and Construction of Externally Bonded FRP Systems for Strengthening Concrete Structures*, 2017).

Three different FRP reinforcement fabrics were used for this research: two CFRP (Carbon Fiber-Reinforced Polymer) and one GFRP fabric (Glass Fiber-Reinforced Polymer); C1, C2 and G1 respectively. A resin “RE” were used with all FRP fabrics, and two different concrete compressive strength, 3500 psi and 6300 psi, were used. Ten walls in total were tested.

Chapter one (1) establishes the research question and goals that allow to obtain reliable results of the impact of the external reinforced with FRP fabrics.

Chapter two (2) presents the literature review, starting with problems that have been observed in TRCW worldwide in a laboratory test or seismic events, studying their

characteristics and failure modes. The second part focuses on reinforcement techniques in reinforced concrete walls (RCW) and ends with contributions of these research and investigations.

Next in Chapter three (3) materials are described, its physics and mechanics properties, main characteristics, and relevant information for this research. The main materials were Concrete, Steel bars and Fiber-Reinforced Polymers (FRP) Fabrics, Carbon and Glass.

Chapter four (4) defines the experimental program, in this section the variables of the research are presented, the constructive process of the specimens and the reinforcement schemes to be used during the tests (showing each scheme design), the instrumentation schemes with LVDTs (linear displacement transducers), also the loading protocol is established; for Unreinforced Walls (wall without external reinforcement) the loading protocol was based on expected load according to interaction diagram.

The results obtained are analyzed in Chapter five (5), showing the loading protocol, failure mode and hysteresis graphics for each wall dividing the results according to RCW strength, high compressive strength (f'c = 6300 psi) and low compressive strength (f'c = 3500 psi). For each RCW strength is presented an envelope of the hysteresis graphics.

Lateral stiffness degradation graphics are generated to assess the RCW behavior as loading cycles process. Energy absorption is also calculated and ends with a comparation between the experimental results and the theoretical calculated according to ACI 440.2R-17.

Finally, in Chapter six (6) presents the conclusions and recommendations of this research.

The present research work was done within the framework of a project that was carried out between La Escuela Colombiana de Ingeniería Julio Garavito and The University of Miami.

1. Research Question and Goals

This chapter contains the research question and the main goals that the study presented in this thesis attempted to address.

1.1 Research Question

Assess behavior under cyclic loads of thin reinforced concrete walls (TRCW) with height to width ratio of 1.0 externally reinforced by fiber reinforced polymers (FRP) fabrics.

1.2 Goals

- Investigate the shear strength enhancement given by the FRP configuration.
- Evaluate the shear strength capacity given by the different FRP systems.
- Evaluate the deformation levels and failures modes in the specimens tested.
- Study the shear strength capacity given by the FRP depending on the concrete strength.
- Calculate and analyze the stiffness degradation and energy dissipation capacity for each specimen.
- Analyze and compare the experimental results and the theoretical values given by the ACI 440.2R-17 equations.

2. Literature Review

2.1 Overview

This chapter presents an overview of existing knowledge on FRP systems for the shear strengthening of RC walls. The literature review begins with the problems found in RC walls subjected to seismic events followed by different reinforcement methods used in investigations and finally, the ACI 440.2R-17 equations to calculate the shear strength provided by the FRP strips. The purpose of this review was to identify the problem of thin reinforced concrete walls (TRCW) and the knowledge gaps in FRP shear reinforcement that the study presented in this thesis attempted to address.

2.2 Seismic behavior of RC Walls

Reinforced concrete walls are one of the most used earthquake resistance systems due to their industrialization (shorter construction times) and economy (lower costs than other structural systems, for example, moment-resisting frames). However; Laboratory tests around the world and earthquakes in countries such as Chile (2010) and New Zealand (2011) have shown that buildings constructed with relatively thin and slender reinforced concrete walls could result in significant damage to heritage and losses of human life. (CEER (Colombian Earthquake Engineering Research Network), 2018).

The industrialized system of thin reinforced concrete walls (TRCW) has demonstrated good resistant earthquake performance in low-rise buildings of up to 3 floors (Carrillo & Alcocer, 2012, 2013). This structural system is mainly used in medium and low social strata in consequence of its low prices, growing significantly despite having limited knowledge about its behavior in a seismic event and few experimental results in laboratory tests. Experimental observations on the seismic performance of thin walls and buildings affected by recent earthquakes such as Maule in Chile 2010 and Christchurch in New Zealand 2011 show that the behavior of slender walls may not be adequate under the action of seismic loads.

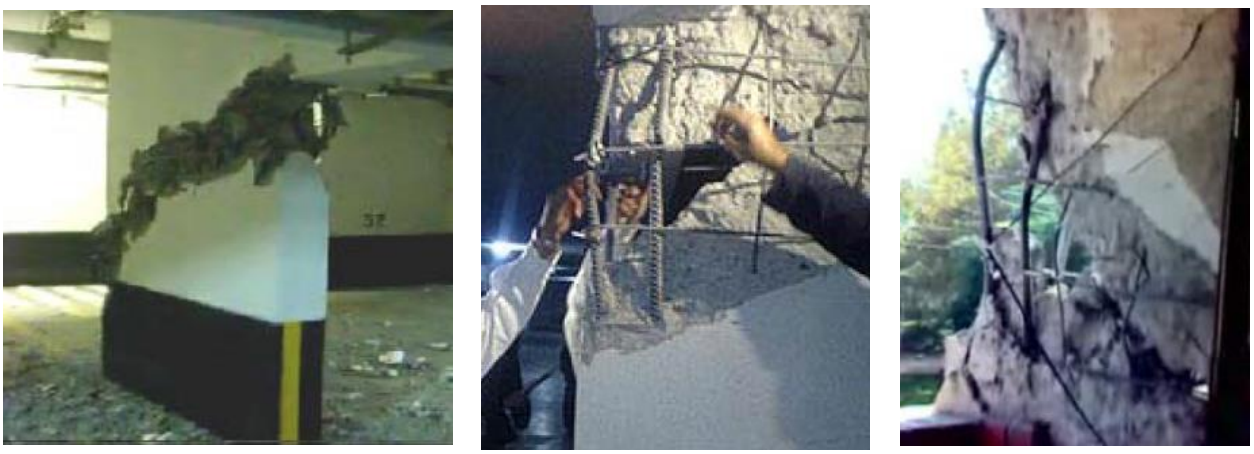

Figure 2.1 – Structural damage during Chile 2010 earthquake
Adapted from (Á. San Bartolomé, 2010)

These failures can be explained due to the lack of confinement in concrete result in fragile failures. In the seismic events, it was also possible to evidenced longitudinal reinforcement out-of-plane lateral instability which could lead to bars rupture. Even where ductile design details were adopted, the expected displacement capacities were not reached and new failure modes were observed (Rosso et al., 2016).

The first evidence of out-of-plane buckling was observed in rectangular walls from some of the laboratory experiments reported by Oesterle (1976), later Goodsir (1985) and Thomsen and Wallace (2004) reported similar behavior in laboratory tests on T-shaped cross-sectional walls in but only until the occurrence of earthquakes in Chile and NZ when evidence of out-of-plane instability was observed in the field (CEER (Colombian Earthquake Engineering Research Network), 2018).

The CEER carried out and investigated over 450 RC walls and found that 48% of the analyzed walls had thickness less than or equal to 100 mm (4 in) and approximately 85% of the walls had thickness less than or equal to 150 mm (6 in).

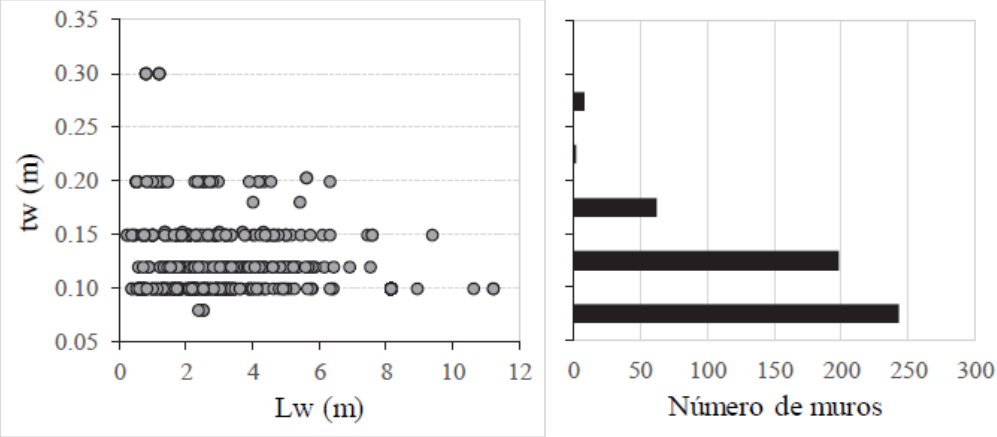

Figure 2.2 – RC Walls thickness distribution

Adapted from (CEER (Colombian Earthquake Engineering Research Network), 2018)

This constructive system (thin reinforced concrete walls) is mainly used in Latin-American countries, however, there are limited information about its behavior under seismic loads (Blandón et al., 2015). Laboratory tests carried out on 80 mm (3.15 in) thick specimens of 1.2 m (47 in) length and 4.5 m (177 in) height showed failure modes characterized by compression at the base and later out-of-plane buckling.

Many of these investigations are framed in modifying design equations or improving the knowledge given by the design codes to consider the limited ductility of this types of walls. As in the case of Colombia that the CEER proposes to modify the NSR-10 (*Reglamento Colombiano de Construcción Sismo Resistente NSR-10*, 2012) by appending "A structural system where seismic resistance and gravity loads are given by reinforced concrete walls of reduced thickness, between 10 and 15 cm, in which confined ends are dispensed with and the vertical reinforcement is arranged in a single layer. The inelastic rotation capacity of this system is limited, as is its energy dissipation capacity".

Other investigations carried out by San Bartolomé (A. San Bartolomé et al., 2007) on 100 mm (4 in) thick specimens of 2.0 m (78.7 in) length and 2.4 m (94.5 in) height and reinforced with electrowelded steel mesh showed similar failures modes characterized for compression at the base and diagonal cracking (see Figure 2.1).

Figure 2.3 – Failure mode RC walls
Adapted from (A. San Bartolomé et al., 2007)

2.3 Reinforcing methods of RC walls.

Considering the possible failures that may occur in the TRCW, it is necessary to establish techniques of reinforcement, repair and rehabilitation in existing structures that could be seriously affected under seismic loads. These techniques are usually focus in the failure modes of shear walls that can be divided into flexural failure and shear failure. (Huang et al., 2020). These behaviors are influenced by different factors, such as the shear span to effective depth ratio and axial compression ratio, (Samad et al., 2016). In engineering practice, shear walls on the bottom floor usually have low aspect ratios that make them susceptible to brittle shear failure (Fintel, 1995).

Omar Ávila, Julián Carrillo and Sergio Alcocer studied the seismic performance of steel fiber reinforced concrete (SFRC) jacketing. The investigation was aimed at rehabilitation of an RC wall reinforced with electrowelded steel mesh. (Ávila et al., 2011). The effectiveness was evaluated by the shear strength, story drift, failure mode and energy dissipation. Although the ACI-318 allowed the use of SFRC to resist shear forces in beams there was no experimental evidence over SFRC jacketing performance on RC walls. The specimens tested were squat RC walls (0.08 x 1.92 x 1.92 m) where the failure mode excepted was diagonal cracking. The specimens were first tested up to severe damage and later rehabilitated with a SRFC jacket around the wall (previously the cracks were closed with epoxy resin).

Lower cracking levels were observed in the rehabilitated specimens, the failure mode was diagonal cracking (shear) in both control and rehabilitated. The rehabilitated/control load rate was 1.46, meaning a 46% more lateral load capacity in the rehabilitated specimen with a SFRC jacket.

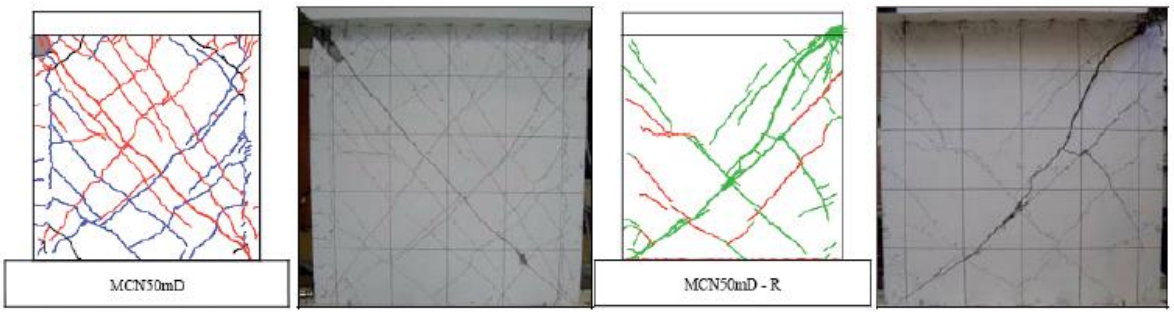

Figure 2.4 – Control and Rehabilitated specimen.
Adapted from (Ávila et al., 2011)

In 2012 Altin, Anil and Kopraman (Altin et al., 2013) studied the hysteretic behavior of RC shear walls strengthened with CFRP (Carbon Fiber-Reinforced Polymers) strips. ACI 440.2R-17 (*American Concrete Institute (ACI) Committee 440. 440.2R-17: Guide for the Design and Construction of Externally Bonded FRP Systems for Strengthening Concrete Structures*, 2017) defines the FRP (Fiber-Reinforced Polymers) system as "the fibers and resins used to create the composite laminate, all applicable resins used to bond it to the concrete substate, and all applied coatings used to protect the constituent materials". The application of these systems has developed rapidly because of its light weight, high strength, linear elasticity and excellent resistance to corrosion (Huang et al., 2020) and ease of application.

Altin's research was based on tested five RC walls with 1.5 aspect ratio, 0.1 x 1.0 x 1.5 m (4 x 40 x 59 in), under cyclic lateral loading, the lateral and vertical reinforcement ratios were 0.0183 and 0.0015 respectively; and 15.5 MPa of concrete compressive strength. Different configurations were tested like X-shaped, horizontal and parallel strips or combinations, all configurations had CFRP anchorage (see Figure 2.5). The shear strength provided by FRP was calculated by equation 1, obtaining at the end of the test that the calculated average shear strengths of the strengthened specimens were 22% higher than that the measured ultimate shear

strength values during the tests. However, the best performance for the improvement of lateral displacement capacity and lateral strength of shear was obtained from the strengthening with lateral strips, Specimen 2 developed a 67% more lateral load capacity than control specimen.

$$V_f = 2 \cdot n \cdot t_f \cdot \sigma_f \cdot d_f \cdot (1 + \cot(\beta)) \cdot sin^2(\beta) \quad (1)$$

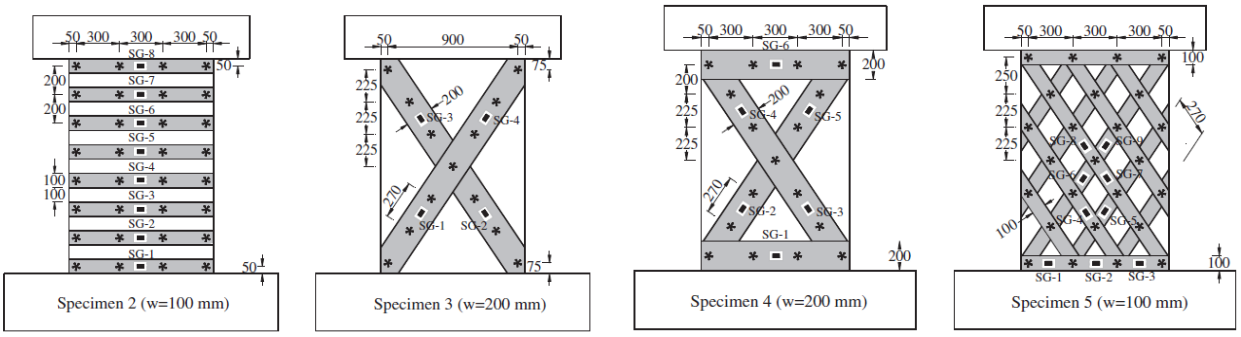

Figure 2.5 – CFRP configuration

Adapted from (Altin et al., 2013)

In 2016 Christidis, Vougioukas and Trezos (Christidis et al., 2016) examined the behavior of strengthened existing non-conforming reinforced concrete shear walls. They tested five specimens (one reference and four strengthened) with 2.0 aspect ratio (0.15 x 0.75 x 1.40 m) and 25 MPa concrete compressive strength. Four different configurations were testes using horizontal steel straps along the height of the wall, with and without steel corner angles. Figure 2.6 shows the reinforcement configurations.

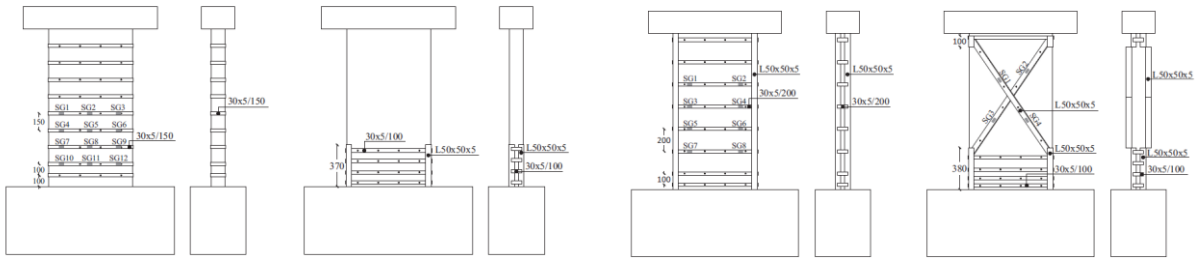

Figure 2.6 – Steel straps configuration

Adapted from (Christidis et al., 2016)

The results showed a better performance of the only horizontal steel straps without steel corner angles specimen, improving by 20% over the maximum load of the control specimen. The investigations above have shown a better performance of horizontal reinforcement to improve the shear strength on RC walls, the orientation of the reinforcement makes it easy to apply and requires less material than other configurations.

Other investigations have used different reinforcement methods to improve the performance of the RC walls under seismic loads like steel-encasing strengthening with slotting, Carbon fiber reinforcement, Steel-bonded reinforcement, Steel-encasing strengthening and Enlarging section strengthening (Christidis et al., 2016; Cruz-Noguez et al., 2015; Dan, 2012; El-Sokkary & Galal, 2013; Jiang et al., 2014; Layssi et al., 2012; Lombard et al., 2000). However, most of these reinforcement methods are invasive (like the anchorages inside the wall) requiring skilled labor and in some cases large amounts of tools.

The FRP systems (carbon, glass and aramid) have become an accepted practice in the civil engineering community due to their lightweight, high tensile strength and ease to install on irregular surfaces (Belarbi & Acun, 2013). Although FRP fabrics have been used to improve the performance of structural members (mostly beams, columns and bridge decks), few studies have examined the behavior on shear walls, focusing mainly on unreinforced masonry walls. In addition, ACI 440.2R-17 (*American Concrete Institute (ACI) Committee 440. 440.2R-17: Guide for the Design and Construction of Externally Bonded FRP Systems for Strengthening Concrete Structures*, 2017) stablishes equations to calculate the shear strength enhancement given by the FRP system.

2.4 ACI 440.2R-17

ACI 440.2R-17 in chapter 13.7 “Strengthening reinforced concrete shear walls” presents design guidelines for the seismic strengthening of reinforced concrete walls (*ACI 440.2R*, 2017). The guide specifies that applying horizontal FRP strips along the height of the wall can increase the shear capacity of reinforced concrete shear walls. Chapter 13.7.3 mentioned above is based on investigations carried out by Haroun and Mosallam (Haroun & Mosallam, 2002), (Haroun et al., 2005), and Khomwan and Foster (Khomwan et al., 2005) and specifies that the shear strength enhancement for a wall section of length L_w in the direction of the applied shear force, with a laminate thickness of on two sides or one side of the wall, can be calculated using:

$$V_f = 2t_f \varepsilon_{fe} E_f d_w \quad \text{(for a two-sided retrofit)} \tag{2}$$

$$V_f = 0.75 t_f \varepsilon_{fe} E_f d_w \ \text{(for a one} - \text{sided retrofit)} \tag{3}$$

Nonetheless, the equations above are based on an investigation conducted by Haroun, Mosallam and Allam (Haroun et al., 2005), in which a horizontal FRP laminate cover one or two sides of the wall (concrete masonry wall), the equations do not take into account the possibility of applying fabrics along the height of the wall. Besides, chapter 11.4 of ACI 440.2R related with the FRP contribution to shear strength in beams and columns stablishes an equation to calculate the shear strength provided by the FRP reinforcement in function of the FRP width, center-to-center spacing, effective depth of FRP and FRP properties.

$$V_f = \frac{A_{fv}\varepsilon_{fe}E_f(sin\alpha + cos\alpha)d_w}{S_f} \quad (4)$$

$$A_{fv} = 2nt_f w_f \quad (5)$$

With the background described above, it is clear the necessity of develop reinforcement methods for thin reinforced concrete walls (TRCW) in order to prevent shear failures during a seismic event, on the other hand FRP composites have shown a great performance strengthening structural elements, reason why the present investigation focused on assess the shear strength improvement in TRCW externally reinforced with FRP horizontal strips, since it was the system that showed the best performance and used less amount of material (evaluating different FRP systems, carbon and glass); and be able to evaluate the equations given by the ACI 440.2R-17 considering the knowledge gap strengthening concrete walls with FRP strips.

3. Experimental Program

3.1 Overview

The experimental program consisted of ten in-plane flexural tests, with applied load at mid-span in order to subject the walls to shear stresses, performed on thin reinforced concrete walls (TRCW) that were designed with deficient shear strength. Two different concrete compressive strengths were used, of low and high strength respectively. Low compressive strength concrete was set at 17.5 MPa (2500 psi) in order to analyze the behavior in existing and old structures. Also chapter 19.2 of ACI 318-19 (*American Concrete Institute (ACI)*, 2019) establishes the minimum concrete strength as 17.5 MPa (2500 psi) and presents a more ductile behavior compared to a higher strength concrete. The high strength concrete was set at 45 MPa (6500 psi) in order to evaluate the behavior of the FRP reinforcement in a more fragile concrete.

Five TRCW were cast in low concrete strength and five on high concrete strength. As reinforcement, externally bonded fiber-reinforced polymer (FRP) fabrics were used, carbon and glass were used since they are the most common and commercial systems. Carbon systems are more rigid and has been more used for reinforcement according to the literature review, glass systems, being more ductile compared to carbon systems, could be more useful in seismic zones since they could absorb more energy. Five TRCW were strengthened with CFRP, three with GFRP, while the remaining were used as unreinforced specimens. The Table 3.6 defines the variables referring to the reinforcement configurations used are defined.

The experimental program began with a material characterization, followed by the design of the thin reinforced concrete walls (TRCW), in order to have the knowledge to establish the reinforcement settings based on the literature review and research objectives.

Once the TRCW design and reinforcement settings were defined, the constructive procedure followed by the external reinforcement with FRP and finally the tests began.

3.2 Materials

A description of the physical and mechanical properties of the materials used in the present investigation is below. These include concrete, reinforcing steel and fiber reinforced polymers (FRP); carbon (CFRP) and glass (GFRP) with the saturating resin, primer and putty coat fillers used in the installation.

3.2.1 Concrete

The walls were cast from two types of hydraulic cement concrete, cylindrical specimens of 100 x 200 mm (4 x 8 in) were cast from each concrete to evaluate its strength at test-day by NTC 673 (ASTM C39) compression tests. The mean value found ($f'c$) was of 17.2 MPa (2500 psi) and 43.5 MPa (6300 psi) respectively.

3.2.2 Reinforcing steel

Steel Grade 420 (Grade 60 in English system) was used for longitudinal and transverse reinforcement. ANNEX C shows the stress – strain curve of #4 bar test according to NTC 2289 (ASTM A706/A706M). The yield stress of the reinforcing steel was 450 MPa (65025 psi).

3.2.3 Fiber reinforced polymers (FRP) fabrics

Three types of fiber reinforced polymers fabrics were used, two CFRP (Carbon Fiber-Reinforced Polymer) and one GFRP fabric (Glass Fiber-Reinforced Polymer); Carbon-1, Carbon-2 and Glass-1 respectively. An "Epoxy-1" resin was used with all FRP fabrics.

- **Carbon-1 (Carbon Fiber-Reinforced Polymer)**: Carbon-1 is a unidirectional carbon fiber fabric with fiber oriented in the 0° direction. It is light weight and resistant to corrosion. Carbon-1 is field laminated using two-part 100% solids and high strength structural adhesives to form a carbon fiber reinforced polymer system. Table 3.1 presents the most representative dimensions and characteristics.

Table 3.1 – Carbon-1 FRP properties

Property or dimension	Experimental Value	Design Value
Thickness	1.02 mm (0.04 in)	1.02 mm (0.04 in)
Color	Black	Black
Weight	600 g/m^2 (17.7 oz/yd^2)	600 g/m^2 (17.7 oz/yd^2)
Tensile strength*	1,339 MPa (194,260 psi)	1,034 MPa (150,000 psi)
Modulus of elasticity*	74,590 MPa (10.8 X 10^6 psi)	73,770 MPa (10.7 X 10^6 psi)
Elongation at break:	1.8%	1.4%

*cured laminate properties

Figure 3.1 – Carbon-1 FRP

own source

- **Carbon-2 (Carbon Fiber-Reinforced Polymer)**: Carbon-2 is a unidirectional carbon fiber fabric with fiber oriented in the 0° direction. It is light weight and resistant to corrosion. Carbon-2 is field laminated using two-part 100% solids and high strength structural adhesives to form a carbon fiber reinforced polymer system. Table 3.2 presents the most representative dimensions and characteristics.

Table 3.2 – Carbon-2 FRP properties

Property or dimension	Experimental Value	Design Value
Thickness	2.03 mm (0.08 in)	2.03 mm (0.08 in)
Color	Black	Black
Weight	1300 g/m^2 (38 oz/yd^2)	1300 g/m^2 (38 oz/yd^2)
Tensile strength*	1,242 MPa (180,130 psi)	1,684 MPa (155,000 psi)
Modulus of elasticity*	98,140 MPa (14.24 X 10^6 psi)	96,527 MPa (14.0 X 10^6 psi)
Elongation at break:	1.27 %	1.1 %

*cured laminate properties

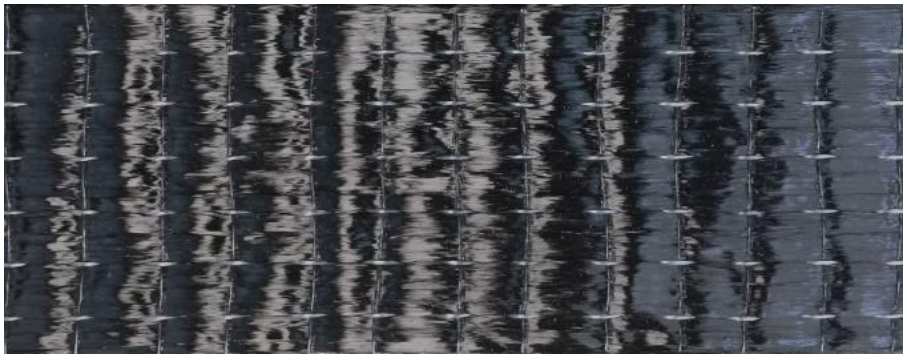

Figure 3.2 – Carbon-2 FRP

own source

- **Glass-1 (Glass Fiber-Reinforced Polymer)**: Glass-1 is a unidirectional carbon fiber fabric with fiber oriented in the 0° direction. It is light weight and resistant to corrosion. Glass-1 is field laminated using two-part 100% solids and high strength

structural adhesives to form a glass fiber reinforced polymer system. Table 3.3 presents the most representative dimensions and characteristics.

Table 3.3 – Glass-1 FRP properties

Property or dimension	Experimental Value	Design Value
Thickness	1.02 mm (0.04 in)	1.02 mm (0.04 in)
Color	White	White
Weight	915 g/m^2 (27 oz/yd^2)	915 g/m^2 (27 oz/yd^2)
Tensile strength*	567.3 MPa (82,280 psi)	487 MPa (70,600 psi)
Modulus of elasticity*	26,680 MPa (3.87 X 10^6 psi)	26,680 MPa (3.87 X 10^6 psi)
Elongation at break:	2.13 %	1.8 %

*cured laminate properties

Figure 3.3 – Glass-1 FRP

own source

- **Epoxy-1 (Epoxy)**: Epoxy-1 is a two component, 100% solids epoxy resin system for high strength composite bonding applications that works as primer, putty coat and saturating resin. Epoxy-1 material is combined with Carbon-1, Carbon-2 and Glass-1 fabrics to provide a wet-layout composite for the strengthening of structural members. Epoxy-1 epoxy may be mixed with fumed silica to produce a putty coat and give it to the wall a finishing coat. Epoxy-1 epoxy should be applied to layers that are free of dust and other contaminates.

3.3 Thin reinforced concrete wall (TRCW) design

For the TRCW design, different aspects were taken into account that would influence directly the design such the expected failure mode, the test setup, how the load would be applied, the hydraulic actuator capacity and the FRP reinforcement.

Since the TRCW should be subjected to shear stresses and the expected failure mode would be a shear failure mainly, the load would be applied at mid-span and the TRCW would have a fixed support at the ends, so the TRCW would be subjected to double shear (Borri et al., 2015). To achieve this the TRCW should have two support beams to anchor it to the slab and to the test frame on top; The high/width rate should be 2 in order to produce a 45° shear crack failure. The reinforcing steel should also be such that bending failure and other typical failures in these walls are avoided.

The TRCW height chosen represents typical wall residential buildings height. To anchor the bottom beam to the strong floor, there are holes in it every 0.5 m (19.7 in). Considering the above, the scheme of the test specimen is presented in Figure 3.6.

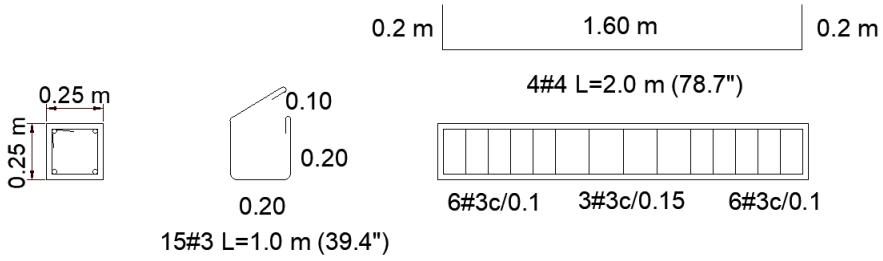

Figure 3.4 - Geometry and reinforcement layout of top beam

own source

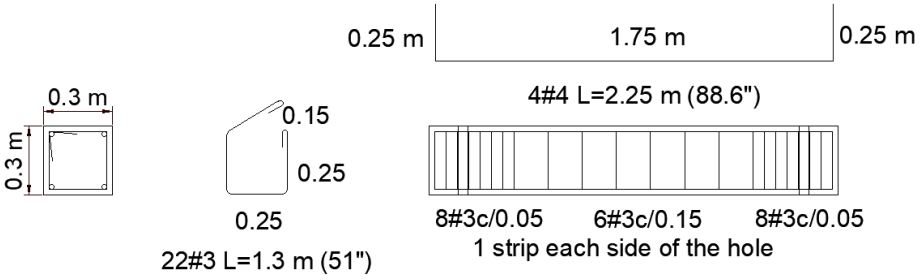

Figure 3.5 - Geometry and reinforcement layout of bottom beam

own source

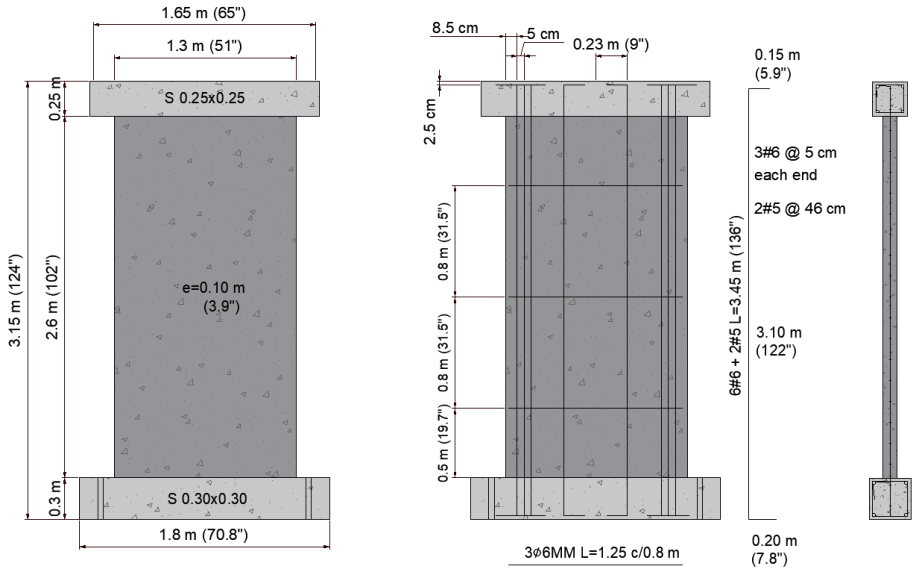

Figure 3.6 - Geometry and reinforcement layout of TRCW

own source

The chosen TRCW was 1.3 m (51”) x 2.6 m (102”) and 0.1 m (3.9”) thick with two support beams as shown in Figure 3.5 and Figure 3.6. The longitudinal reinforcement consists of eight reinforcing steel bars, three #6 bars at each end spaced 5 cm (2”) apart and one #5 bar at 23 cm (9”) from the center. The transverse reinforcement consists of three D 6.0 drawn wire spaced 0.8 m (31.5”) apart as shown in Figure 3.6.

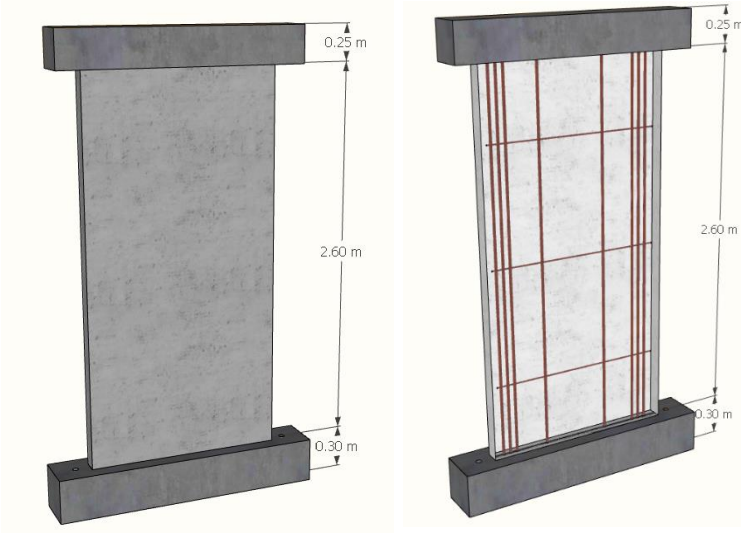

Figure 3.7 – 3D Details of TRCW

own source

Once the details of the wall and the characteristics of the materials were known, the next step was to calculate the capacity of the wall and determine the expected failure mode. The wall interaction diagram was made for this purpose, the input data used to create it is shown in Table 3.4.

Table 3.4 – Input data for interaction diagram

Property or dimension		**Value**
Maximum concrete strain	ε_{cu}	0.0030
Yield steel strain	ε_y	0.0021
Modulus of elasticity of steel	E_y	200 GPa (29x10^3 ksi)
Wall length	l_w	1.30 m (51”)
Wall thickness	t_w	0.1 m (3.9”)
Reinforcement covering	d'	0.085 m (3.3”)
Effective wall length	d_w	1.215 m (47”)
Concrete strength	f'_c	17.2 MPa (2500 psi) & 43.5 MPa (6300 psi)
Longitudinal steel yield strength	f_{yl}	450 MPa (65 ksi)
Wall height	h_w	2.60 m (102”)
Transverse steel yield strength	f_{yt}	450 MPa (65 ksi)

With the input data presented previously, the interaction diagram for the wall was made; the result for each concrete strength is shown below in Figure 3.8:

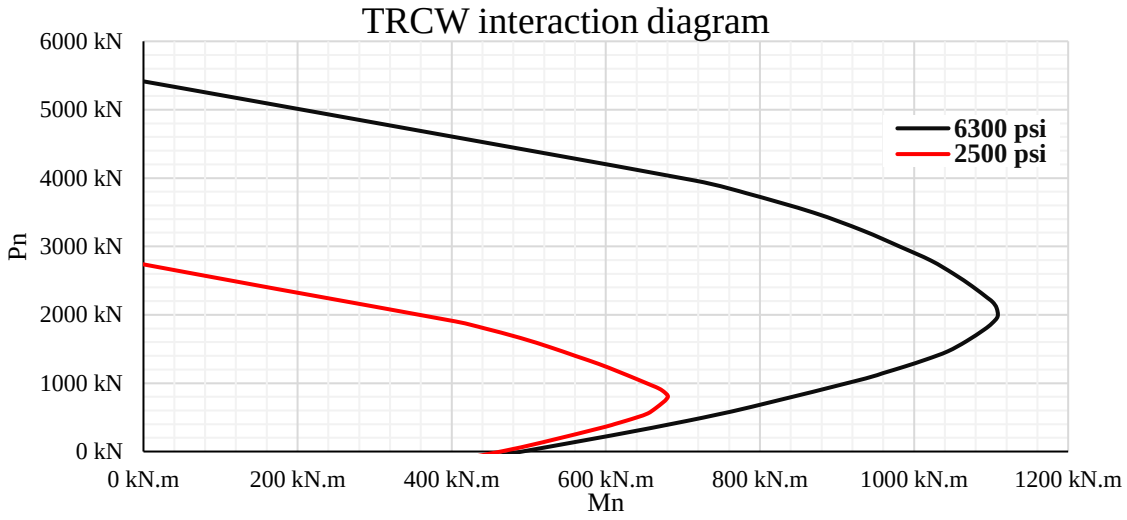

Figure 3.8 – TRCW interaction diagram

Own source

The moment at which there is no axial force (pure flexion) is obtained from Figure 3.8 for each concrete strength, **494.5 kN.m** (364.7 kip.ft) for f'c 2500 psi and **527 kN.m** (388.7 kip.ft) for f'c 6300 psi. To calculate the wall's capacity and its failure mode, its shear and bending strength was first calculated as follow:

Different authors propose different equations to calculate the shear strength of reinforced concrete walls based on the concrete and steel contribution, one of them is the equation given by the ACI 318-19, equation 18.10.4.1 (*American Concrete Institute (ACI) Committee 318. Building Code Requirements for Structural Concrete and Commentary*, 2019).

$$V_n = \left(\alpha_c \lambda \sqrt{f'_c} + \rho_t f_{yt}\right) \cdot t_w \cdot l_w \tag{6}$$

Where:

$$\alpha_c = 0.17\ for\ {}^{h_w}/_{l_w} \geq 2.0\ (MPa) \quad (7)$$

$$\lambda = 1.0\ for\ normal\ concrete$$

Replacing the values in equation (1):

$$V_n = \left(0.17 * 1.0 * \sqrt{17.2\ MPa} + 0.00035 * 500\ MPa\right) \cdot 100\ mm \cdot 1300\ mm/1000$$

$$V_n = 114.4\ kN\ (25.7\ kip)$$

The value obtained with the ACI equation could be conservative when M/VL < 0.5 (squat walls) and can be increased by 1.43 in order to get a measure similar than the tested (Sánchez-Alejandre & Alcocer, 2010). The M/VL for the specimen tested is 0.5 and can be considered as a squat wall. Therefore, $V_R = 163.6\ kN\ (36.8\ kip)$. The same procedure is performed for the high concrete strength (43.5 MPa, 6300 psi), resulting in a shear resistance of $V_R = 242.1\ kN\ (54.4\ kip)$

As already mentioned, the test setup consisted of a double end fixed element with a mid-span load (see Figure 3.9). The element would be subjected to double shear force, therefore, the shear resistance previously calculated should be multiplied by two to know the force to be applied to the element, $\boldsymbol{P_L = 328\ kN}$ (73.7 kip), $\boldsymbol{P_H = 484.2\ kN}$ (108.8 kip) for the low and high concrete compressive strength, respectively. These are the forces that must be applied to the TRCW to produce shear failure.

With the shear failure known force, the moment at which it would occurs is calculated. From the element fixed at both ends, the maximum moment produced by the force is $M_L = \frac{P_L \cdot h_w}{8}$, replacing in the equation for both concrete strength, the results are $\boldsymbol{M_L = 106.6\ kN.m}$ (78.6 $kips.ft$) and $\boldsymbol{M_H = 157.4\ kN.m}$ (116.1 $kips.ft$).

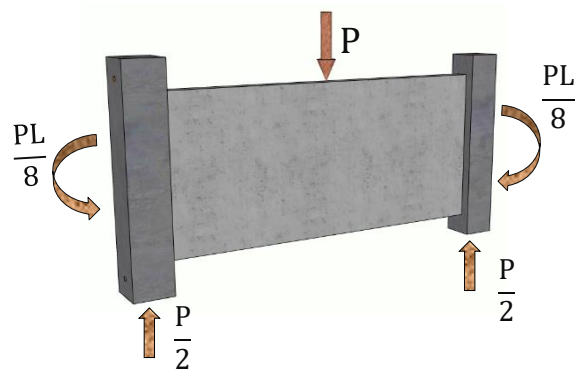

Figure 3.9 – Model element fixed at both ends with point load.

Own source

Table 3.5 shows the TRCW expected failure mode for the dimensions and reinforcement chosen. This behavior was verified with the tests.

Table 3.5 – Comparation between resistant and produced moment

Concrete strength	Resistant moment	Produced moment by maximum shear force	Expected failure mode
17.2 MPa (2500 psi)	494.5 kN.m	106.6 kN.m	Shear failure
43.5 MPa (6300 psi)	527.0 kN.m	157.4 kN.m	Shear failure

3.4 Reinforcement settings

Table 3.6 shows the variables of the experimental study based on the literature review, ten TRCW were tested in total, five of high strength (43.5 MPa / 6300 psi) and five of low strength (17.2 MPa / 2500 psi). Since the shear capacity was the property to be improved by the reinforcement, the literature review for wall's reinforcement recommends an FRP horizontal orientation in order to achieve this. ACI 440.2R-17 (ACI 440.2R, 2017, p. 42) mentions that "applying horizontal FRP strips along the height of the walls can increase the shear capacity of reinforced concrete shear walls", according to this the reinforcement settings was set in

horizontal FRP fabrics. The ACI 440.2R-17 does not specify horizontal FRP fabrics for wall's strength reinforcement, instead specify FRP laminate covering one or two faces of the concrete wall according to Haroun et al (Haroun et al., 2005). For this investigation, several FRP fabrics along the height were proposed to be able to see the cracks and that the fabrics could cross most cracks. Some of the benefits of this proposed reinforcement settings are the lower price in reinforcement material, workforce compared to an FRP laminate, and the possibility to carry out a post-earthquake assessment.

According to above, a single reinforcement setting was proposed, the reinforcement setting consisted of seven FRP fabrics of 7.6 cm (3 in) width and 1.3 m (51 in) length separated 35.6 cm (14 in) center-to-center. The difference between the various specimens was the fabrics arrangement (one or two sides) and an extra characteristic in the two sides setting that consisted in wrapping the FRP around the corner.

Table 3.6 – Variables of the experimental study

Wall ID	FRP system	f'c	Fabric arrangement
L-0	-	17.2 MPa	-
L-G1-1	G1 + R1	17.2 MPa	1 side
L-G1-2	G1 + R1	17.2 MPa	2 sides
L-C1-1	C1 + R1	17.2 MPa	1 side
L-C1-2	C1 + R1	17.2 MPa	2 sides
H-0	-	43.5 MPa	-
H-C1-1	C1 + R1	43.5 MPa	1 side
H-C2-1	C2 + R1	43.5 MPa	1 side
H-C1-1-90	C1 + R1	43.5 MPa	1 side*
H-G1-2-90	G1 + R1	43.5 MPa	2 sides*

*Wrapped around the corner

3.4.1 Test matrix

All TRCW were uniquely identified based on their strength, FRP system used, number of sides reinforced and an additional relevant characteristic. The format used to name it is:

X-YY-Z-W

Where X is concrete strength, YY is the FRP system used on the sides of the wall, Z is the number of reinforced sides and finally, W is the additional relevant characteristic of the reinforcement used. Table 3.7 presents a description of the nomenclature parameters and

Figure 3.10 shows the 3D model of the reinforcement settings.

Table 3.7 – Description of the nomenclature parameters

Parameter	Description	Identification
Concrete strength	f'c = 17.2 MPa (2500 psi)	L
	f'c = 43.5 MPa (6300 psi)	H
FRP system	Carbon-1	C1
	Carbon-2	C2
	Glass-1	G1
Number of reinforced sides	One side	1
	Two sides	2
Additional characteristic	Wrapped around the corner	90

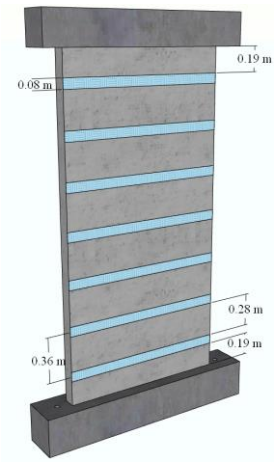

L-C1-1

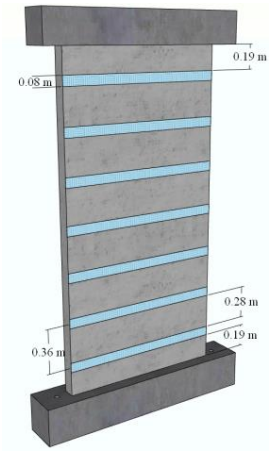

L-C1-2

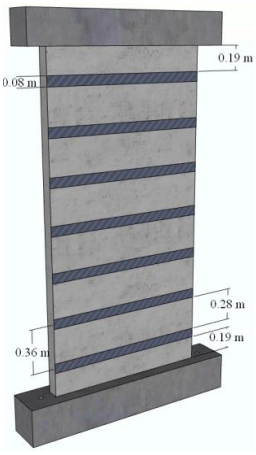

L-C1-1

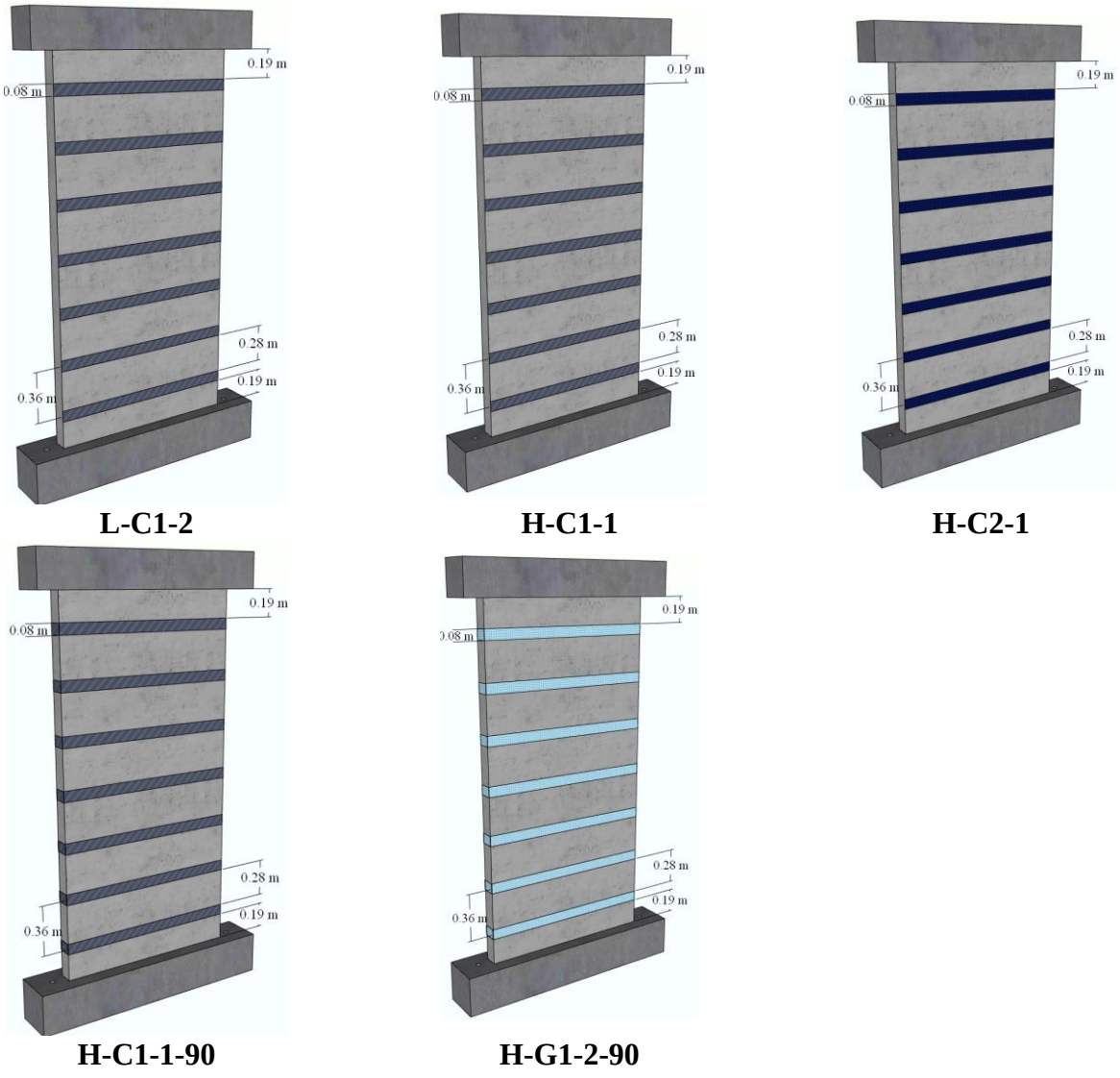

Figure 3.10 – 3D model of the reinforcement settings.

Own source

3.5 Constructive procedure

The constructive procedure was based on the wall design in Figure 3.6. The construction began with the bottom beam construction and finalized with the top beam. Figure 3.11 show de process.

(a) Bottom beam reinforcement

(b) Bottom beam formwork

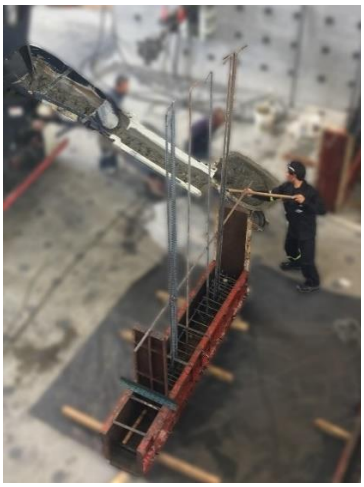

(c) Bottom beam casting

(d) Bottom beam with reinforcement

(e) Wall formwork

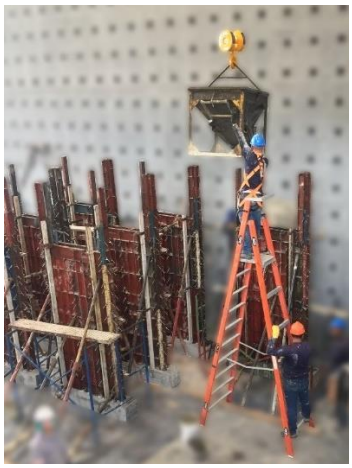

(f) Wall casting

(g) Stripped wall

(h) test specimen

Figure 3.11 – Constructive procedure.

Own source

During constructive process, cylindrical specimens were casted to evaluate the mechanical properties of the concrete.

3.6 Reinforcement procedure

According to the reinforcement setting established in chapter 3.4 for each TRCW, the reinforcement procedure is explained as follows, taking into account the FRP manufacturer's recommendations.

3.6.1 Surface preparation

To ensure of an adequate bonding between the concrete surface and the wet-layout composite for the strengthening of the TRCW, the concrete surface should be dry and exhibit an open pore structure. To achieve this, the ICRI No. 310.2R guidelines were followed (*ICRI Guideline No. 310.2R*, 2013). All bond inhibiting materials should be removed from the surface before the FRP application. The putty coat can be used to fill holes in the concrete surface and to smooth the uneven surfaces of the concrete.

A concrete surface profile (CSP) number 3 (CSP 3) in accordance with the ICRI No. 310.2R is aimed. In order to obtain this, open pore structure a grinder polishing machine with a diamond cup wheel and a type 11 cup wheel for granite is used for flat surfaces and curved surfaces respectively.

Figure 3.12 presents the concrete surface before and after the polishing process, afterward, the surface was cleaned up and all the materials like dust, grease and waxes were removed.

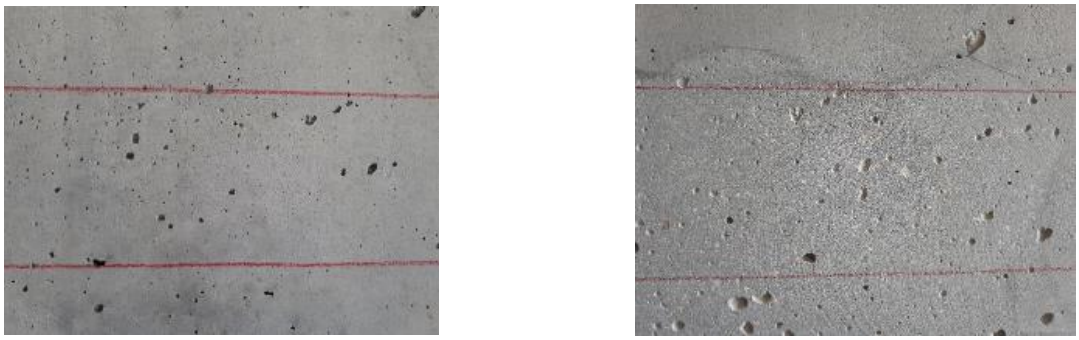

(a) (b)

Figure 3.12 –surface preparation (a) before (b) after polishing process

Own source

3.6.2 Primer, Putty coat and Saturant Epoxy preparation

For the epoxy preparation, the manufacturer's recommendations were followed. The mixing process begin premixing Part A for 2 minutes, then, Part B is added to Part A and finally both are mixed for 3 minutes until a uniform mixture is obtained. Part A represents 70.9% and Part B 29.1% of the total mix. As said before, fumed silica (FS) can be added to thicken the epoxy and be used as putty coat. According to with the manufacturer, the maximum ratio by volume is 1.5 of fumed silica to 1 part of resin. Table 3.8 shows the coverage rates depending on its use.

Table 3.8 – Epoxy coverage rates

Use	Description	Amount
As a primer	Concrete	5.5 m^2/L (225 ft^2/gal)
As putty coat (with FS)	Filler	1.0 m^2/L (60 ft^2/gal)
As saturant	Carbon-1	1.5 m^2/L (60 ft^2/gal)
	Carbon-2	1.0 m^2/L (40 ft^2/gal)
	Glass-1	1.5 m^2/L (60 ft^2/gal)

The amounts required for the L-C1-1 specimen are explained below:

1. Epoxy uses: Primer (5.5 m^2/L), Putty coat (1.0 m^2/L) and Saturant (1.5 m^2/L).
2. Set the FRP amount, 1.3 m * 0.076 m * 7 = **0.69 m^2** of FRP fabric.
3. With the FRP amount and epoxy coverage rate, each use volume can be calculated: Primer = 0.1261 L, Putty coat = 0.4623 L and Saturant = 0.4623 L.
4. Next, the fumed silica amount is calculated establishing a ratio by volume of 1.25. The fumed silica is mixed with the epoxy to produce the putty coat, as the putty coat amount was 462.3 mL, the fumed silica amount is **260 mL** and the Part A + Part B used with it is 205 mL.
5. Finally, the total Part A + Part B amount are calculated adding 126.1 mL + 205 mL + 462.3 mL = 794 mL. Considering each percentage of the total amount for Part A and Part B, **563 mL** and **231 mL** are obtained respectively.

3.6.3 FRP application

After calculating the epoxy amounts were calculated, the next step consisted in placing the FRP reinforcement considering the manufacturer's recommendations.

1. Surface preparation: once the stripes where the FRP reinforcement will go have been marked, polishing process is carried out to obtain a CSP-3, See Figure 3.13.

Figure 3.13 – surface preparation

Own source

2. Epoxy preparation: With the quantities of epoxy in Part A, Part B and silica fumed determined, mixing was carried out according to times mixing described in chapter 3.6.2. Figure 3.14 shows the process.

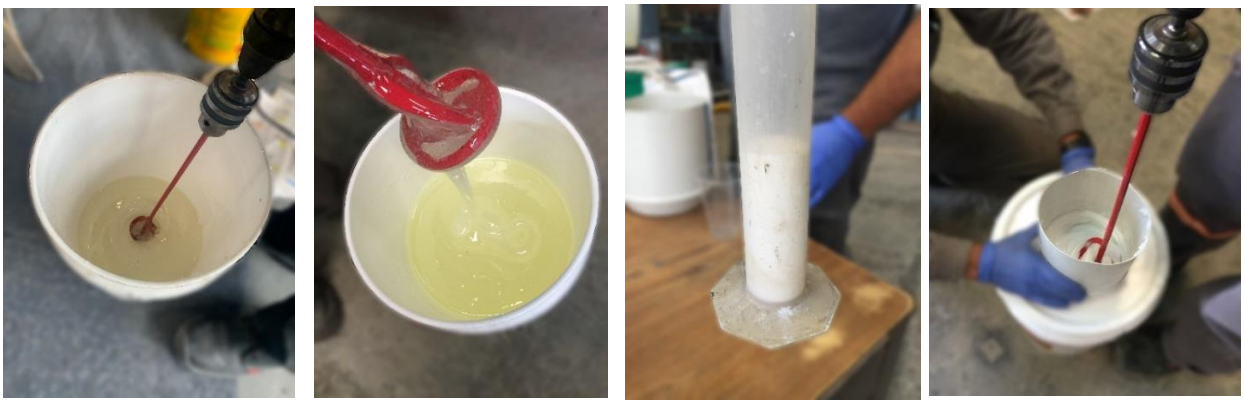

(a) (b) (c) (d)

Figure 3.14 – Epoxy mixing process (a) Part A (b) Resin-1 (c) Silica fumed (d) Putty coat

Own source

3. Putty coat, Primer and FRP fabric saturation: The small imperfections of the concrete surface are filled with the putty coat epoxy. Afterward, the concrete was primed by applying a thin layer of the primer epoxy using a nap roller (see Figure 3.15 (a)) . The saturant epoxy was poured over to the FRP fabric and is extended using a brush, using a rib roller all air pockets are removed and thus a full saturation of the fabric is achieved (see Figure 3.15 (b)).
4. FRP fabric installation: Manually following the guidelines previously drawn the FRP fabrics were placed on the surface and finally, with the help of flexible spatulas, the FRP fabrics were seated and the excess epoxy material was removed (see Figure 3.15 (c), (d)).

(a) (b) (c) (d)

Figure 3.15 – (a) Priming of the surface (b) Saturating of the FRP fabric (c) FRP application (d) FRP applicated

Own source

The same procedure was carried out for the reinforcement of the other specimens, considering the necessary dosage depending on the number of FRP fabrics to be used and their thickness.

3.7 Theoretical capacity

The theoretical capacity of the TRCW specimens was calculated based on the ACI 440.2R – 17 guidelines (*ACI 440.2R*, 2017) as mentioned above.

$$\emptyset V_n^* = \emptyset(V_c + V_s + \psi_f V_f) \geq V_u \tag{8}$$

$$V_f = \frac{A_{fv}\varepsilon_{fe}E_f(sin\alpha + cos\alpha)d_w}{S_f} \tag{9}$$

$$A_{fv} = 2nt_f w_f \tag{10}$$

A_{fv} is the area of FRP external reinforcement and as it can be appreciated it is multiplied by 2 because ACI 440.2R considers FRP reinforcement on both sides of the beam only. When there is only one-sided reinforcement in this investigation, the A_{fv} calculation won't be affected

by 2. ψ_f is a recommended additional reduction factor for FRP shear reinforcement, however this factor does not take into account the possibility of one-sided scheme and is based on beam reinforcement. This reduction factor to calculate the FRP shear contribution will not be considered.

The effective strain in FRP reinforced attained at failure (ε_{fe}) is calculated according to chapter 11.4.1 of the guide, which is based in Triantafillou (Triantafillou, 1998). In this investigation the equations limits will not be considered, especially for the high concrete compression strength specimens.

$$\varepsilon_{fe} = \kappa_v \varepsilon_{fu} \leq 0.004 \tag{11}$$

The bond-reduction coefficient (κ_v) can be computed from eq. 11.

$$\kappa_v = \frac{k_1 k_2 L_e}{11900 \varepsilon_{fu}} < 0.75 \ \ (SI) \tag{12}$$

Where:

$$L_e = \frac{23300}{(n t_f E_f)^{0.58}} \ (SI) \tag{13}$$

$$k_1 = \left(\frac{f'_c}{27}\right)^{2/3} \ (SI) \tag{14}$$

$$k_2 = \frac{d_w - 2L_e}{d_w} \ (for\ two\ sides\ bonded)$$
$$k_2 = \frac{d_w - L_e}{d_w} \ (for\ U - wraps) \tag{15}$$

ACI 440.2R-17 specifies that the maximum clear spacing between the FRP shear strips must be limited to the minimum of one-fifth of the overall length of the wall, three times the

thickness of the wall, or 18 in (457 mm). Table 3.9 shows the input data to calculate the shear strength provided by the FRP for the different TRCW reinforcement settings. The FRP's properties are in Table 3.1, Table 3.2 and Table 3.3 for Carbon-1, Carbon-2 and Glass-1 respectively.

Table 3.9 – Input data to calculate the shear strength provided by the FRP.

Property		Value	
Wall height	h_w	2.6 m	102.4 in
Wall length	l_w	1.3 m	51.2 in
Wall thickness	t_w	0.1 m	3.9 in
Low concrete strength	f'_c	17.2 MPa	2500 psi
High concrete strength		43.5 MPa	6300 psi
Shear strength of the wall for low f'c	V_{RE}	320 kN	71.9 kip
Shear strength of the wall for high f'c		500 kN	112.4 kip
Effective depth of the shear wall	d_w	1.112 m	43.8 in
Width of FRP reinforcing plies	w_f	0.076 m	3.0 in
Center-to-center spacing of FRP	S_f	0.36 m	14.17 in

Annex B contains the design calculation for the FRP contribution for L-C1-1 specimen and Table 3.10 shows the shear strength provided by the FRP reinforcement for each TRCW specimen.

Table 3.10 – Theoretical capacities of TRCW's reinforcement.

Specimen ID	$P_{nc,u}$ [kN (kip)]	ΔP_{nFRP} [kN (kip)]	$P_{n,FRP}$ [kN (kip)]	%G
L-0	328 (73.7)	--	--	--
L-G1-1	320 (71.9) *	44 (9.9)	364 (81.8)	14%
L-G1-2	320 (71.9) *	88 (19.8)	408 (91.7)	28%
L-C1-1	320 (71.9) *	72 (16.2)	392 (88.1)	23%
L-C1-2	320 (71.9) *	142 (31.9)	462 (103.9)	44%
H-0	484 (108.8)	--	--	--
H-C1-1	500 (112.4) *	132 (29.7)	632 (142.1)	26%
H-C2-1	500 (112.4) *	206 (46.3)	706 (158.7)	41%
H-C1-1-90	500 (112.4) *	138 (31.0)	638 (143.4)	28%
H-G1-2-90	500 (112.4) *	174 (39.1)	674 (151.5)	35%

Pnc,u = Theoretical capacity unstrengthened specimen.
ΔPnFRP = Contribution of the FRP to the shear capacity of the wall.
Pn,FRP = Theoretical capacity strengthened specimen.
* = The theoretical capacity of unstrengthened specimen was calculated according to its failure mode and concrete strength at day test.
%G = Gain over control.

3.8 Loading protocol

In order to develop the load control protocol of the unreinforced specimens, the shear strength of the TRCW was taken as a reference according to the results of chapter 3.3 for each concrete strength, the expected shear strengths are V_R = 332 kN for the low concrete strength and V_R = 484 kN for the high concrete strength.

The load control protocol of the unreinforced specimens consisted of three initial steps of 25%, 50% and 75% of the expected load with only one cycle of each step, starting cycle 100% each step would have three cycles and increments of 10% of the expected load until its failure. The test speed was set in 900 kg/s (1.98 kip/s), Figure 3.16 shows the graphic applied load in % P_{nc} vs time.

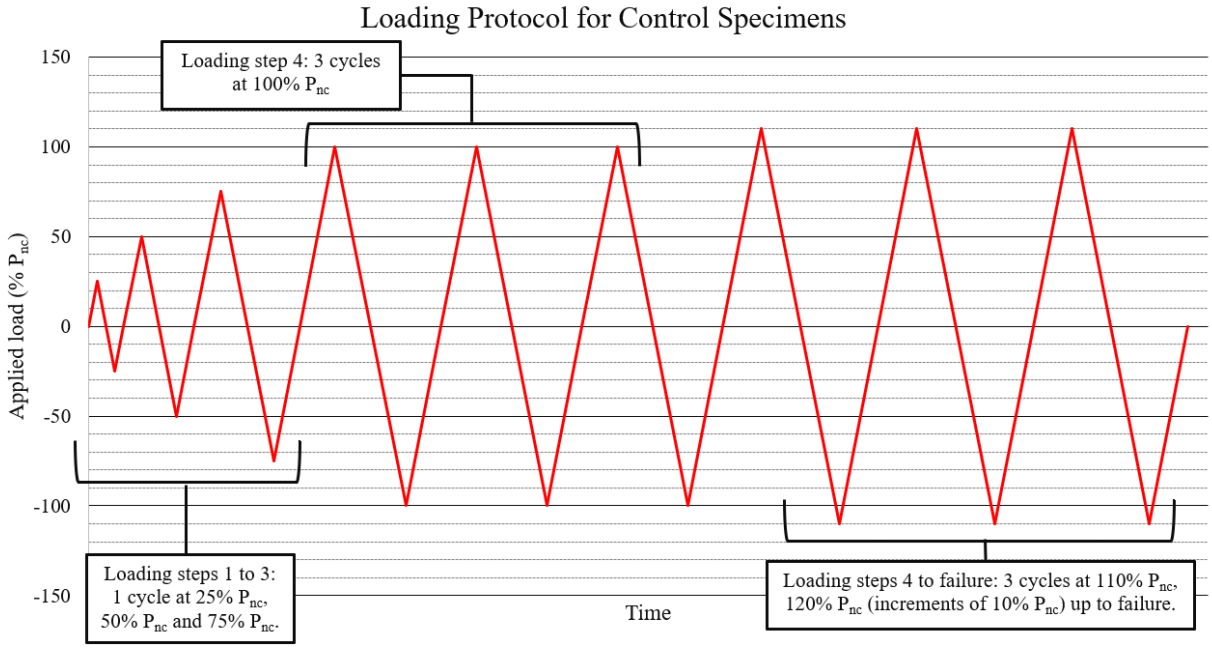

Figure 3.16 – Loading protocol for Unreinforced Specimens.

Own source

Based on the TRCW's real capacities after testing on the unreinforced specimens; the loading protocol for the reinforced specimens (see Figure 3.17) was divided in two (an hybrid control); the first one, a force control, based on the maximum load capacity record on the unreinforced specimens (320 kN for low concrete strength TRCW and 500 kN for high concrete strength TRCW, see chapter 4.3), performing steps at 25%, 50% and 75% P_{nc}. Afterward, as in the unreinforced specimens load control, a four step with three cycles at 100% P_{nc} and four more steps performing fixed increments depending on the FRP reinforcement setting. Finally, taking as a reference the maximum displacement value recorded in the eighth step, the control is changed to displacement control, performing increments of 25% μ_u up to failure. The reason for this loading protocol was to evaluate ductility, the steps allow evaluate the energy absorption capacity and the tension-compression cycles allow assess the behavior under seismic cases.

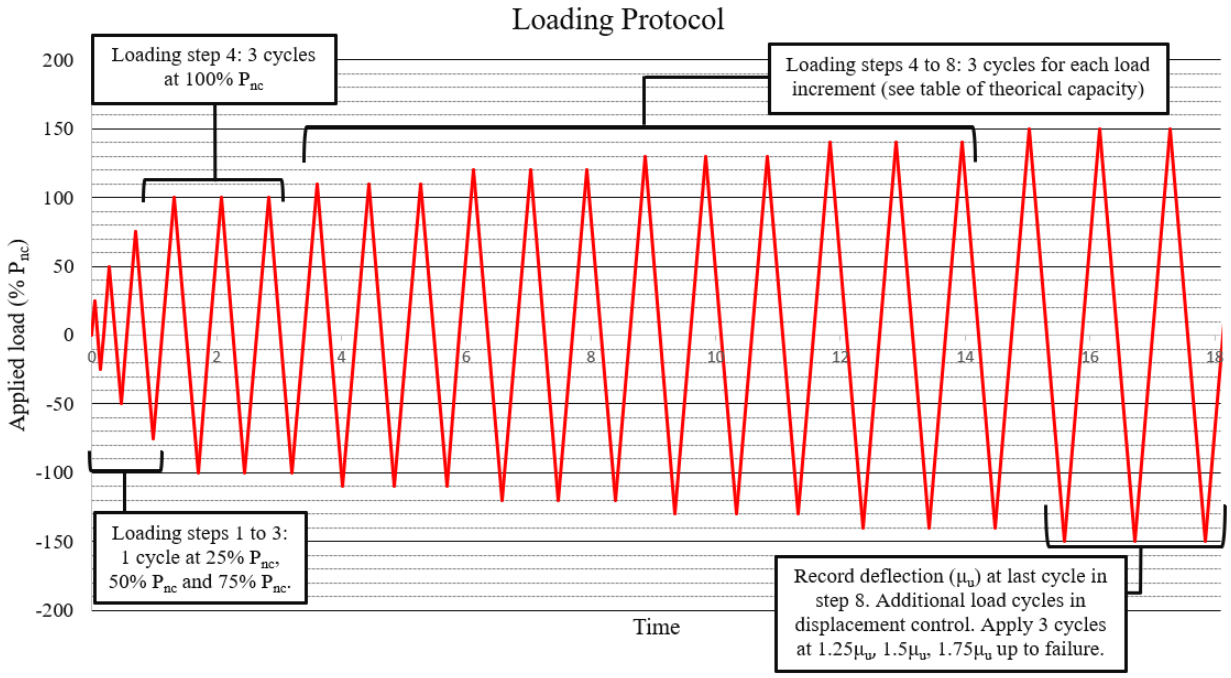

Figure 3.17 – Loading protocol for Reinforced Specimens.

Own source

3.9 Test setup and instrumentation

The test setup consisted of a loading frame connected to the wall reaction in the structure's laboratory of the Escuela Colombiana de Ingeniería Julio Garavito. The load application was made by an MTS hydraulic actuator of 1000 kN (225 kips) capacity. Figure 3.18 shows a 3D model of the test setup. The instrumentation was carried out through five linear displacement transducers (LVDTs) located at different points on the wall as shown in Figure 3.20. LVDT-1 was located at half-height, LVDT-2 was located at upper beam, LVDT-3 at the bottom of the wall, LVDT-4 at bottom beam and LVDT-5 diagonally behind the wall.

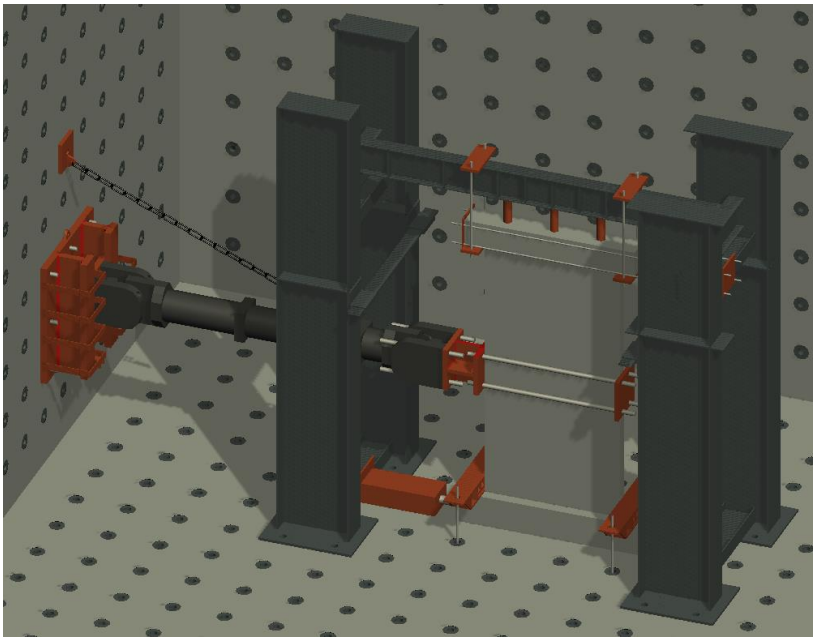

Figure 3.18 – 3D model of the test setup.

Own source

Figure 3.19 –Test setup.

Own source

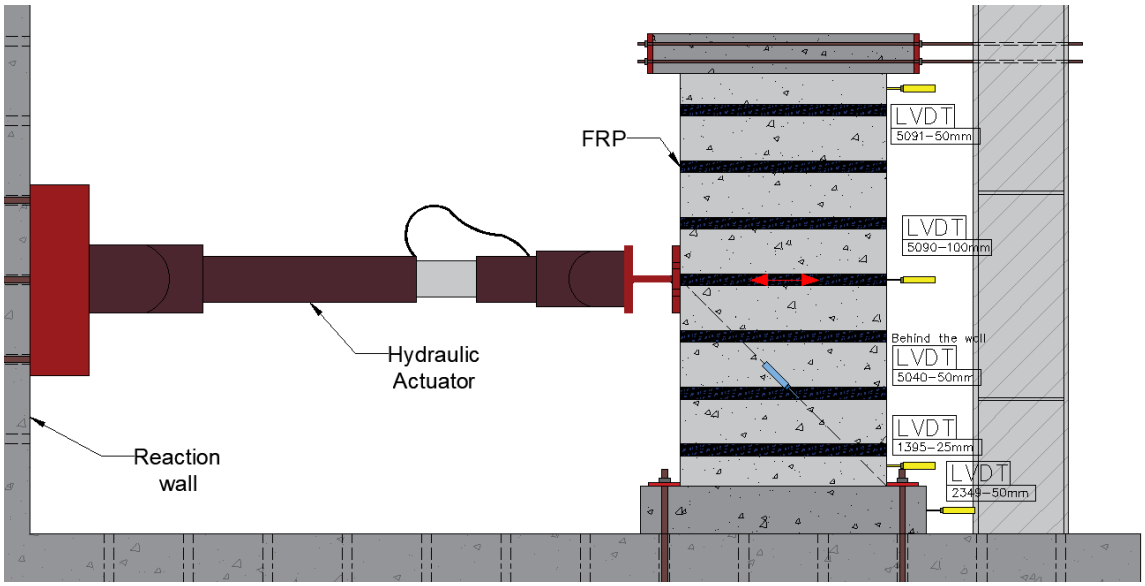

Figure 3.20 – Typical instrumentation of the test.

Own source

In the laboratory, during the execution of the tests, an average relative humidity of 75% and a temperature of 16 ° C were registered.

4. Results and Analysis

4.1 Overview

This chapter presents the ten specimens tested experimental results. First, a classification of the failure mode of each specimen is made, then, the load capacity of the TRCWs is presented and with the results registered during the test, the hysterical response is graphed. Based on these results, the stiffness degradation and ductility analysis are carried out. Finally, a comparison with ACI 440.2 – 17 theoretical equations.

4.2 Load capacity of the walls in cyclical tests

Table 4.1 shows the maximum load results and the failure mode for each TRCW. The results are divided in maximum tension load and maximum compression load in order to carry out an analysis considering its failure mode. Table 4.1 also shows the experimental/theoretical load rate.

For the low strength unreinforced wall, the experimental lateral load was 4% lower than expected. However, this calculation can be considered with a good degree of precision and taking the values given by Sánchez and Alcocer (Sánchez-Alejandre & Alcocer, 2010) as a good exercise to obtain shear strength in concrete walls.

Table 4.1 – Results in TRCW specimens

Specimen ID	Lateral tension displacement mm (in)	Lateral compression displacement mm (in)	Maximum tension load kN (kip)	Maximum compression load kN (kip)	Maximum theoretical load kN (kip)	exp/the failure	Failure mode
L-0	10.2 (0.40)	10.3 (0.41)	314 (71)	**314 (71)**	328 (73.7)	**0.96**	Shear failure
L-G1-1	15.7 (0.62)	18.9 (0.74)	430 (97)	**330 (74)**	364 (81.8)	**0.91**	Shear followed by FRP delamination
L-G1-2	10.1 (0.40)	8.4 (0.33)	**404 (91)**	404 (91)	408 (91.7)	**0.99**	Shear followed by FRP delamination
L-C1-1	12.9 (0.51)	12.9 (0.51)	**377 (84.7)**	355 (79.8)	392 (88.1)	**0.96**	Shear followed by FRP delamination
L-C1-2	5.0 (0.20)	8.4 (0.33)	390 (88)	**573 (129)**	462 (103.9)	**1.24**	Shear followed by FRP delamination
H-0	10.0 (0.39)	7.3 (0.29)	**488 (109)**	382 (86)	484 (108.8)	**1.01**	Shear failure
H-C1-1	10.1 (0.39)	8.7 (0.34)	**803 (180)**	670 (150)	632 (142.1)	**1.27**	Shear followed by FRP delamination
H-C2-1	8.6 (0.34)	10.8 (0.43)	**891 (200)**	718 (161)	706 (158.7)	**1.26**	Shear followed by FRP delamination
H-C1-1-90	7.4 (0.29)	6.3 (0.25)	**800 (179)**	638 (143)	638 (143.4)	**1.25**	Shear followed by FRP delamination
H-G1-2-90	9.6 (0.38)	7.5 (0.30)	**834 (200)**	664 (149)	674 (151.5)	**1.24**	Shear followed by FRP delamination

Based on the maximum experimental load the designs of the reinforced specimens with FRP were established, with 320 kN force being the standard for a low strength unreinforced wall, making the appropriate corrections for the concrete strength changes in the wall on the test day. For the one-sided reinforcement specimens, the L-G1-1 specimen reached a maximum load 18% greater than expected, however the failure load was equal to 91% of the expected theoretical, this load was reached in the compression cycle, the same cycle in which the failure with detachment of the bands occurs as analyzed in chapter 4.3.2. For L-C1-1 specimen, the maximum load was presented in the tension cycle, being 96% of the theoretical load, in this cycle the failure of the wall was also presented by delamination and detachment of the lower bands as discussed in chapter 4.3.4.

For the two-sided reinforcement specimens without wrapping around the corner, the L-G1-2 specimen supported a load equal to the theoretical expected both in the tension and compression cycles, the failure load was located in tension cycle where the wall reached a displacement of 10.1 mm. Finally, the L-C1-2 specimen resisted a load 24% higher than expected, this load was reached in the compression cycle in which the failure occurs. All the specimens reached higher capacities than the unreinforced specimen as shown in Figure 4.1, with L-G1-1 being the one that gained the least resistance, with 5% higher than the unreinforced specimen and L-C1-2 the one that had the highest with 82 %. From this initial analysis it can be seen that the specimens reinforced with carbon fiber (with higher modulus and lower elongation at break) showed better behavior in terms of maximum load supported, however, the specimens reinforced with fiberglass showed higher displacements before failure, which will be analyzed in chapter 4.4. The single-sided reinforced specimens presented lower strengths than expected calculated using ACI 440.2R-17, these strength overestimations will be discussed in chapter 4.7.

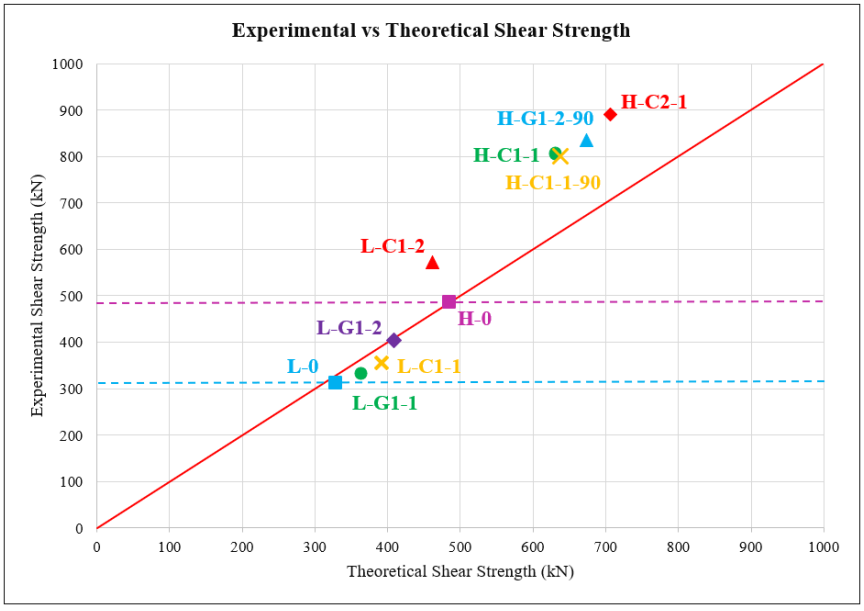

Figure 4.1 – Experimental vs theoretical shear strength.

Own source

The high strength unreinforced specimen reached a load 1% higher than the expected one. Based on the maximum experimental load the designs of the reinforced specimens with FRP were established with 500 kN load being the standard for a high strength unreinforced wall, making the appropriate corrections for the concrete strength changes in the wall on the test day. For the one-sided reinforcement specimens, the H-C1-1 specimen showed a maximum load 27% higher than the theoretical expected (and 65% higher with respect to the unreinforced specimen), the fall occurred in the tension cycle when the actuator was pulling the wall. The H-C2-1 specimen which the elastic modulus of the reinforcement was higher than C1, reached a maximum load in the tension cycle 26% higher than the theoretical expected (and 83% higher with respect to the unreinforced specimen). The H-C1-1-90 specimen which had a similar reinforcement with H-C1-1, with the only difference this was wrapped around the corner, achieved a maximum load in the tension cycle 25% higher than the theoretical expected (and 64% higher with respect to the unreinforced specimen). Compared with H-C1-1 specimen, the difference was minimum. However, H-C1-1-90 was stiffer, this will be analyzed in chapter 4.4.

Finally, the H-G1-2-90 specimen, which presented the greatest reinforcement, reached a failure load in the tension cycle 24% higher than the expected (and 71% higher with respect to the unreinforced specimen).

All reinforced specimens reached loads higher than the unreinforced specimen as can be seen in Figure 4.1, being specimens H-C1-1 and H-C1-1-90 which less strength gained (64% with respect to the unreinforced specimen) and the H-C2-1 specimen which more strength gained with 83%. From this initial analysis, all the specimens showed resistance on average 26% higher than expected.

Table 4.2 shows the relation between the gained strength vs the volume of reinforcement used, showing that there is no direct relationship between this rate and the type of FRP used, this implies that it may depend more on the configuration, resistance of the substrate and reinforcement configuration.

Table 4.2 – Gained strength to reinforcement volume ratio

Specimen ID	Maximum load kN (kip)	Gained strength kN (kip)	Reinforcement volume cm^3 (in^3)	GS / RV kN/cm^3
L-0	314 (71)	--	--	--
L-G1-1	330 (74)	10 (2.3)	707 (43.2)	0.01
L-G1-2	404 (91)	84 (18.9)	1415 (86.3)	0.06
L-C1-1	377 (85)	57 (12.8)	707 (43.2)	0.08
L-C1-2	573 (129)	253 (56.9)	1415 (86.3)	0.18
H-0	488 (109)	--	--	--
H-C1-1	803 (180)	303 (68.1)	707 (43.2)	0.43
H-C2-1	891 (200)	391 (87.9)	1408 (85.9)	0.28
H-C1-1-90	800 (179)	300 (67.4)	816 (49.8)	0.37
H-G1-2-90	834 (200)	334 (75.1)	1523 (93.0)	0.22

(Ávila et al., 2011), (Altin et al., 2013) and (Christidis et al., 2016) reached load capacities up to 46%, 22% and 20% of the unreinforced wall, respectively. On average 32.4% and 70.5% of the unreinforced wall for the low concrete compression strength and high strength, respectively. Showing a great performance compared to the literature review researches.

4.3 Failure mode

A description of the failure mode for each TRCW specimen is made and a relevant behavior during the test is described for a better understanding of the results obtained. All the tests were carried out until the integrity of the TRCW was compromised.

4.3.1 L-0 Specimen

Figure 4.2 shows the failure mode for L-0 Specimen. The failure mode was shear failure (diagonal cracking) as expected. The TRCW's failure occurred in the second compression cycle (the hydraulic actuator was pushing) at 100% P_{nc} and was concentrated in the lower half of the wall, however, the double shear behavior was visible.

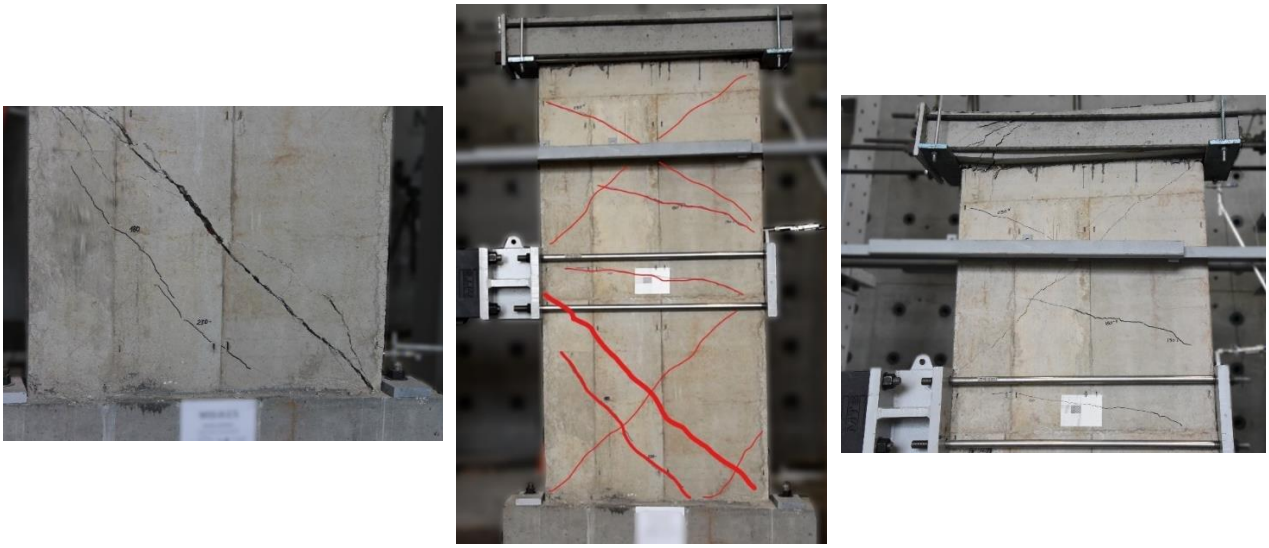

Figure 4.2 – Failure mode L-0 Specimen.
Own source

4.3.2 L-G1-1 Specimen

Figure 4.3 shows the failure mode for L-G1-1 Specimen. The main failure crack was a diagonal cracking (shear) in the lower half of the wall, followed by FRP delamination. The second fabric was totally detached from the surface and the third one was partially detached where the crack passed, the first fabric presented pumping in the crack zone but never detached full. A concrete volume came off at the end of the third fabric at the same time this detached. The TRCW specimen exceeded the load control and reached a load at 1.75 μ_u up to failure. The

failure occurred when the hydraulic actuator was pushing in the compression cycle, the specimen maintained its integrity during test.

Figure 4.3 – Failure mode L-G1-1 Specimen.

Own source

4.3.3 L-G1-2 Specimen

Figure 4.4 shows the failure mode for L-G1-2 specimen. The main failure crack was diagonal cracking (shear) in the lower half of the wall, followed by FRP delamination. All fabrics presented pumping before delamination. The specimen also presented crushing in the applying load zone. The TRCW specimen exceeded the load control and reached a load at 1.75 μ_u up to failure. The failure occurred when the hydraulic actuator was pulling in the tension cycle, the specimen maintained its integrity during test.

Figure 4.4 – Failure mode L-G1-2 Specimen.

Own source

4.3.4 L-C1-1 Specimen

Figure 4.5 shows the failure mode for L-C1-1 Specimen, the main failure crack was double diagonal cracking (double shear), followed by FRP delamination and concrete crushing in the applying load zone. The first crack came out at 75% P_{nc} in the tension cycle but as the cycles increased the main failure was coming out in the compression cycles. The TRCW specimen presented multi-cracking before failure. All fabrics came off where failure crack went across (the third fabric was the first one to delaminated), but none were completely detached. The failure was presented when the hydraulic actuator was pushing in the compression cycle, the specimen maintained its integrity during test.

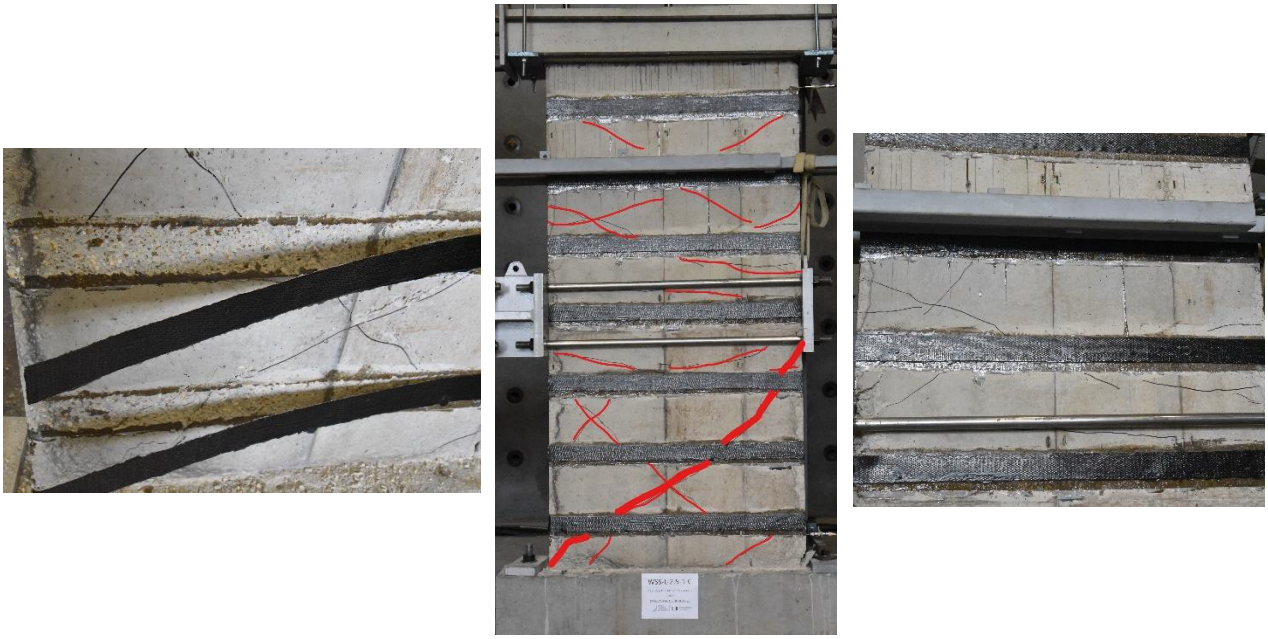

Figure 4.5 – Failure mode L-C1-1 Specimen.

Own source

4.3.5 L-C1-2 Specimen

Figure 4.6 shows the failure mode for L-C1-2 Specimen. The main failure crack was diagonal cracking (shear), followed by FRP delamination in the zones where the crack went across. The third fabric in the back side didn't present detaching, none were completely detached. The first crack came out at 50% P_{nc} in the compression cycle but wasn't the main crack. The specimen presented a multi-cracking behavior before failure. The failure ocurred when the hydraulic actuator was pushing in the compression cycle, the specimen maintained its integrity during test.

Figure 4.6 – Failure mode L-C1-2 Specimen.
Own source

4.3.6 H-0 Specimen

Figure 4.7 shows the failure mode for H-0 Specimen. As expected, the failure mode was shear failure (diagonal cracking), the TRCW's failure occurred in the tension cycle (the hydraulic actuator was pulling) and was concentrated in the lower half of the wall. However, the double shear behavior was visible. At 50% P_{nc} the first crack was observed, then as the force was increasing, the crack was opening and several more cracks were showing up. Finally, at the failure force the main crack was located at the place where the first crack was observed.

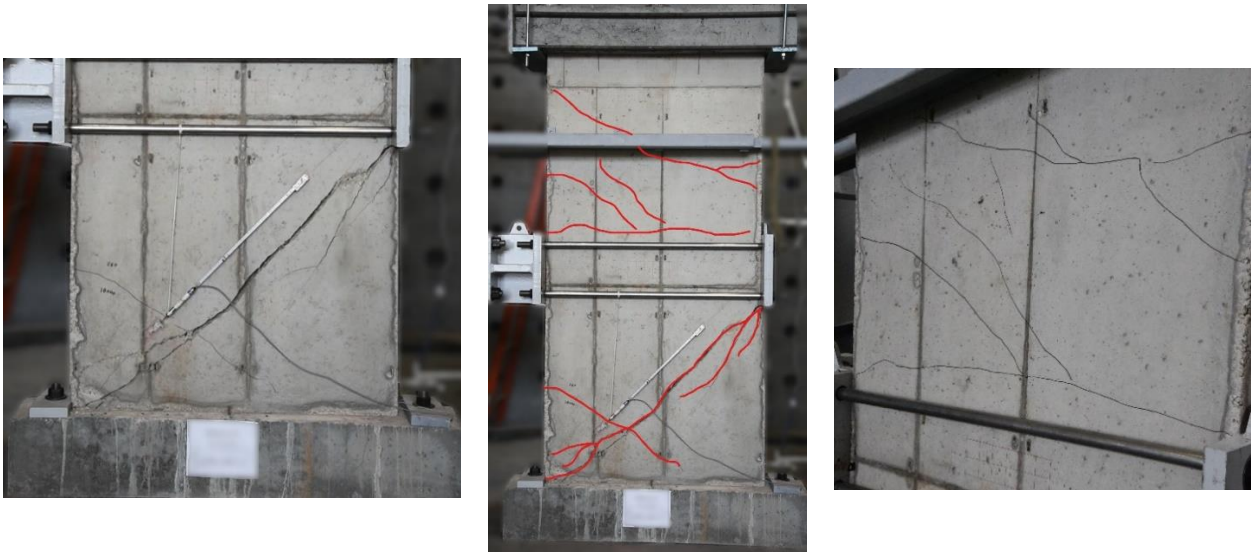

Figure 4.7 – Failure mode H-0 Specimen.

Own source

4.3.7 H-C1-1 Specimen

Figure 4.8 shows the failure mode for H-C1-1 specimen. The main failure crack was a diagonal cracking (shear), followed by FRP delamination in the zones where the crack went across, the fifth and seventh fabric also presented rupture. The first crack came out at 50% P_{nc} in the tension cycle coinciding with the main crack. The specimen presented a multi-cracking behavior before failure. The failure was presented when the hydraulic actuator was pulling in the tension cycle, the specimen maintained its integrity during test with only detachment of a small concrete volume at the third fabric end.

Figure 4.8 – Failure mode H-C1-1 Specimen.

Own source

4.3.8 H-C2-1 Specimen

Figure 4.9 shows the failure mode for H-C2-1 Specimen. The main failure crack was a diagonal cracking (shear), followed by FRP delamination in the zones where the crack went across, none were detached. The first crack came out at 50% P_{nc} in the tension cycle coinciding with the main crack. The specimen presented a multi-cracking behavior before failure. The failure occurred when the hydraulic actuator was pushing in the compression cycle, the specimen maintained its integrity during test with concrete crushing in the applying load zone.

Figure 4.9 – Failure mode H-C21-1 Specimen.

Own source

4.3.9 H-C1-1-90 Specimen

Figure 4.10 shows the failure mode for H-C1-1-90 specimen. The main failure crack was a diagonal cracking (shear), followed by FRP delamination in the zones where the crack went across, the fabrics were the crack went across were detached, taking with them a small volume of concrete. The fifth fabric also presented rupture. The first crack came out at 50% P_{nc} in the tension cycle but was not the main crack. The specimen presented a multi-cracking behavior before failure. The failure happened when the hydraulic actuator was pulling in the tension cycle, the specimen maintained its integrity during test.

Figure 4.10 – Failure mode H-C1-1-90 Specimen.

Own source

4.3.10 H-G1-2-90 Specimen

Figure 4.11 shows the failure mode for H-G1-2-90 specimen. The main failure crack was a diagonal cracking (shear), followed by FRP delamination in the zones where the crack went across, the third fabric in the back side was detached and presented rupture in the wrapping corner and the first one also presented rupture in the same zone. The first crack came out at 50% P_{nc} in the compression cycle but was not the main crack. The specimen presented a multi-cracking behavior before failure. The failure happened when the hydraulic actuator was pulling in the tension cycle, the specimen maintained its integrity during test.

Figure 4.11 – Failure mode H-G1-2-90 Specimen.

Own source

4.4 Hysterical response

Figure 4.12 shows the load-displacement hysteresis curve for L-G1-1 specimen tested under cyclical lateral load applied at half the height, graphic show applied load vs mid-span displacement and its peak lateral load is shown. Annex A contains the remaining hysteresis curves. “The load-displacement hysteretic loop is a critical index of seismic performance, inside which area can be used as a measure of the energy dissipation capacities” (Shen et al., 2017 p. 7).

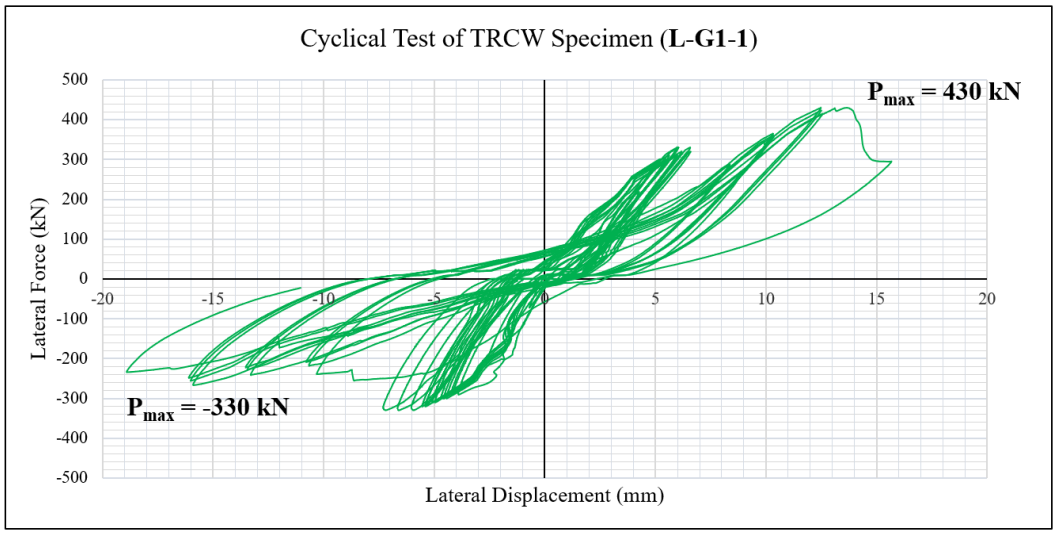

Figure 4.12 – Applied load versus mid-span displacement cycles for L-G1-1 specimens

Own source

To make a comparison between the graphics, Figure 4.13 and Figure 4.14 show the hysterical cycles envelopes for the low concrete strength TRCW and high concrete strength TRCW, respectively. These curves would be used to evaluate load resistant, deformation capacities, ductility and stiffness degradation.

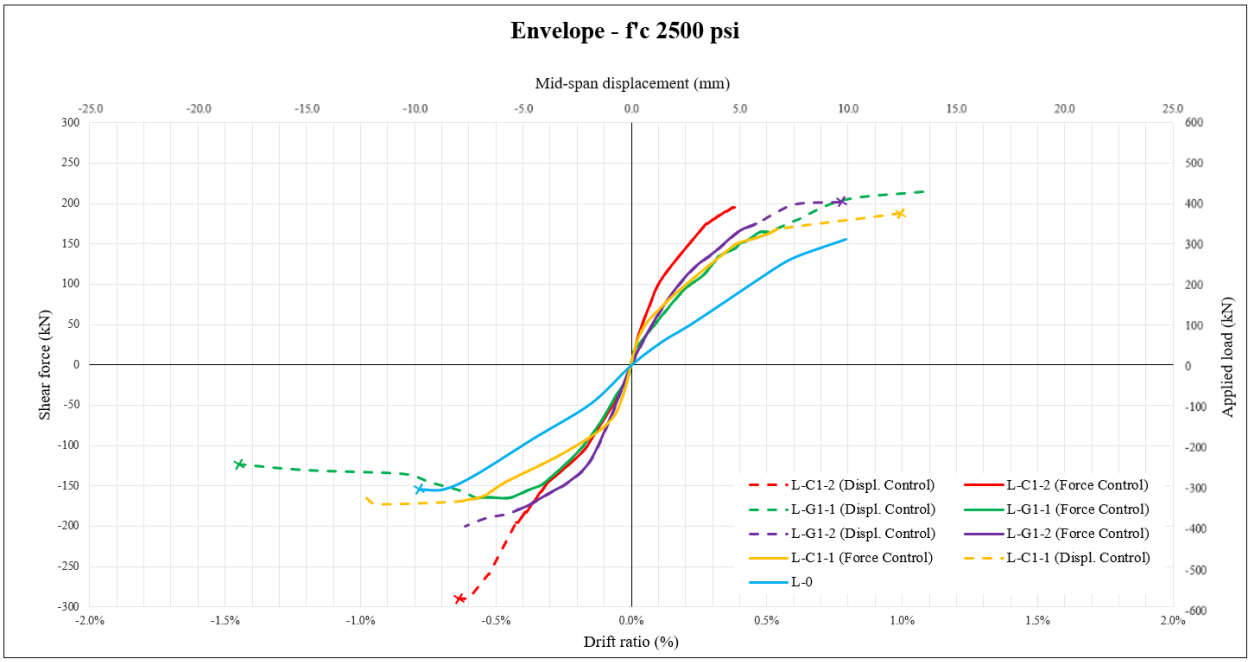

Figure 4.13 – Envelope - f'c 2500 psi.
Own source

Figure 4.13 shows that most specimens failed at compression cycle except for L-G1-2 which failed at tension cycle; all reinforced specimens showed a shear strength improvement respect with the unreinforced specimen. As mentioned, the expected failure mode was shear failure and according to the TRCW specimen design the expected shear failure was 328 kN and the flexural failure was expected at 1500 kN, reason why the unreinforced specimen did not present a drop in load but increased up to failure, presented a fragile and sudden failure. The reinforced specimens showed a stiffening due to the horizontal fabrics that did not allow shear cracks open.

Figure 4.14 also presented the same behavior for the unreinforced specimen (H-0), showing a stiffening in the reinforced specimens, all specimens failed at tension cycle. The graphic clearly shows the improvement in the shear strength given by the FRP strips.

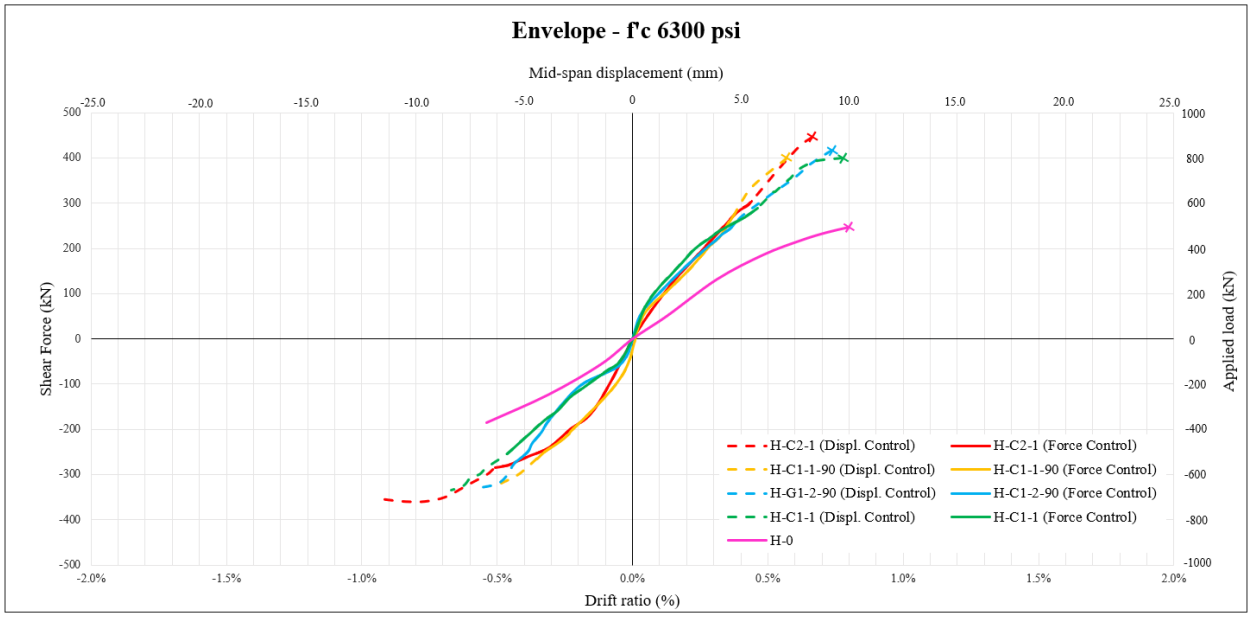

Figure 4.14 – Envelope - f'c 6300 psi.

Own source

Related to deformation capacities, the unreinforced specimens reached a mid-span displacement of 10.3 mm and 10.0 mm before failure for low strength and high strength specimens respectively (see Table 4.1 and Figure 4.15). "Ductility is one of the major issues of concern in achieving the widespread acceptance of FRP-reinforced concrete structures in practice" (Zhou et al., 2009). However, as mentioned, the expected failure mode was a fragile failure (shear failure) and FRP to be a brittle material would rupture suddenly, therefore, it is not possible to calculate a ductility level due to the lack of a defined elastic zone, consequently, a deformation capacity analysis will be carried out in order to assess the reinforced specimens capacity of limit the width of the cracks or conversely, allow a higher width before failure.

The L-G1-1 specimen reached a deformation at failure 83% higher than the unreinforced specimen and the L-G1-2 specimen presented a mid-span displacement almost the same as the unreinforced specimen (10.1 vs 10.3 mm). Both specimens were reinforced with GFRP in which was expected higher levels compared with the specimens reinforced with CFRP that reached a deformation at failure of 126% and 81% of the unreinforced specimen for the L-C1-1 and L-C1-2 respectively. Specimens reinforced with glass FRP (G1) achieved higher levels of deformation capacity than carbon specimens (C1) with the same reinforcement configuration. Specimens reinforced in one side also reached higher levels of deformation at failure than specimens reinforced in both sides, this can evidence the stiffening given by the FRP that in both sides also showed higher load capacities.

Results in the high strength specimens showed that H-C1-1 and H-G1-2-90 were near to the H-0 specimen's deformation at failure. H-C2-1 reached a higher shear strength capacity and lower displacement compared with H-C1-1, C2 system had higher elasticity modulus, therefore, it was expected this behavior. H-C1-1-90 that was wrapped around the corner, showed similar load capacities as H-C1-1, however, the wrapping did not allow the cracks to open as width as the H-C1-1 specimen, thus deformation at failure was lower. H-G1-2-90 specimen, which had the higher reinforcing, showed low displacement values compared to the other glass specimens that reached displacement higher than the unreinforced specimens. This can be explained because of the reinforcement configuration where the fabrics were wrapping around the corner in both sides limiting the cracks opening.

As evidenced in chapter 4.3 no FRP fabric failed because of rupture, instead the main failure mode was delamination. This failure mode is closely related to the bond effectiveness, chapter 11.4.1.2 of ACI 440.2R-17 stablished that "FRP systems that do not enclose the entire

section have been observed to delaminate from the concrete before the loss of aggregate interlock of the section" (Triantafillou, 1998). The bond effectiveness can be related to the FRP area fraction, elastic modulus, FRP configuration and substrate strength. In relation to the substrate strength in the graphic can see that as higher the concrete strength higher the shear strength enhancement.

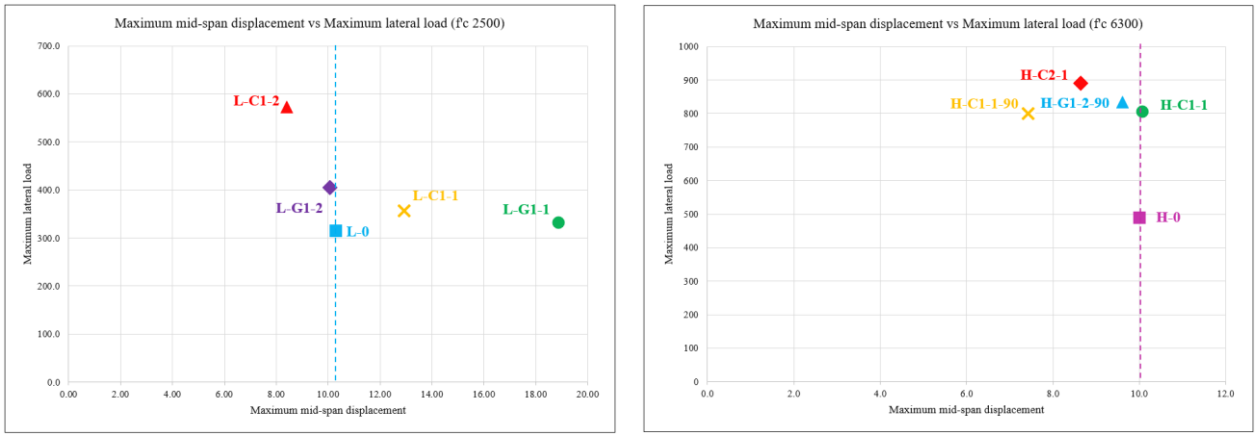

a) f'c 2500 b) f'c 6300

Figure 4.15 – Maximum mid-span displacement vs maximum lateral load.

Own source

4.5 Stiffness degradation

The stiffness of the TRCW corresponds to each of the loops that make up the hysteresis cycles presented in Figure 4.12 and in Annex A. This slope was calculated as the relationship between applied load and mid-span displacement in each loop. Figure 4.16 and Figure 4.17 show the lateral stiffness degradation for low strength and high strength specimens respectively.

The actual stiffness values for RC walls are far below those values calculated with elastic properties (Antoniades et al., 2007). The stiffness values for the specimens was calculated with the secant stiffness, defined as the ratio between the load and current displacement at each loading cycle (Shen et al., 2017).

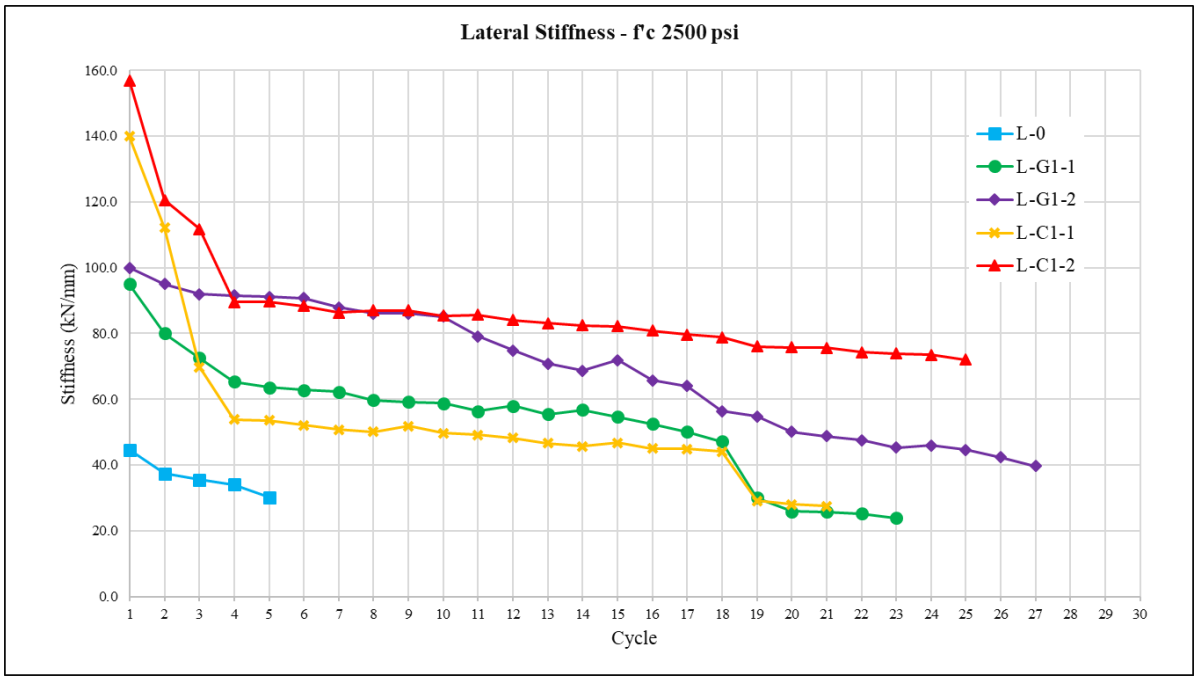

Figure 4.16 – Stiffness degradation, low strength specimens (f'c 2500 psi).
Own source

Because of the failure mode, the low transverse reinforcement and high longitudinal reinforcement, the initial secant stiffness was too different for the reinforced specimens and the unreinforced specimen. For the unreinforced specimen, the initial secant stiffness was 45 kN/mm and decreased 32.3% up to failure. The specimens reinforced with GFRP increased the initial secant stiffness to 100 kN/mm, stiffening the reinforced specimen in 24% compared with the unreinforced specimen, L-G1-1 had higher degradation compared with L-G1-2 specimen as expected. In 19th cycle a drop in load was evidenced as a result of the protocol change. L-G1-1 specimen decreased its stiffness in 75% up to failure and L-G1-2 stiffness decreased in 60%.

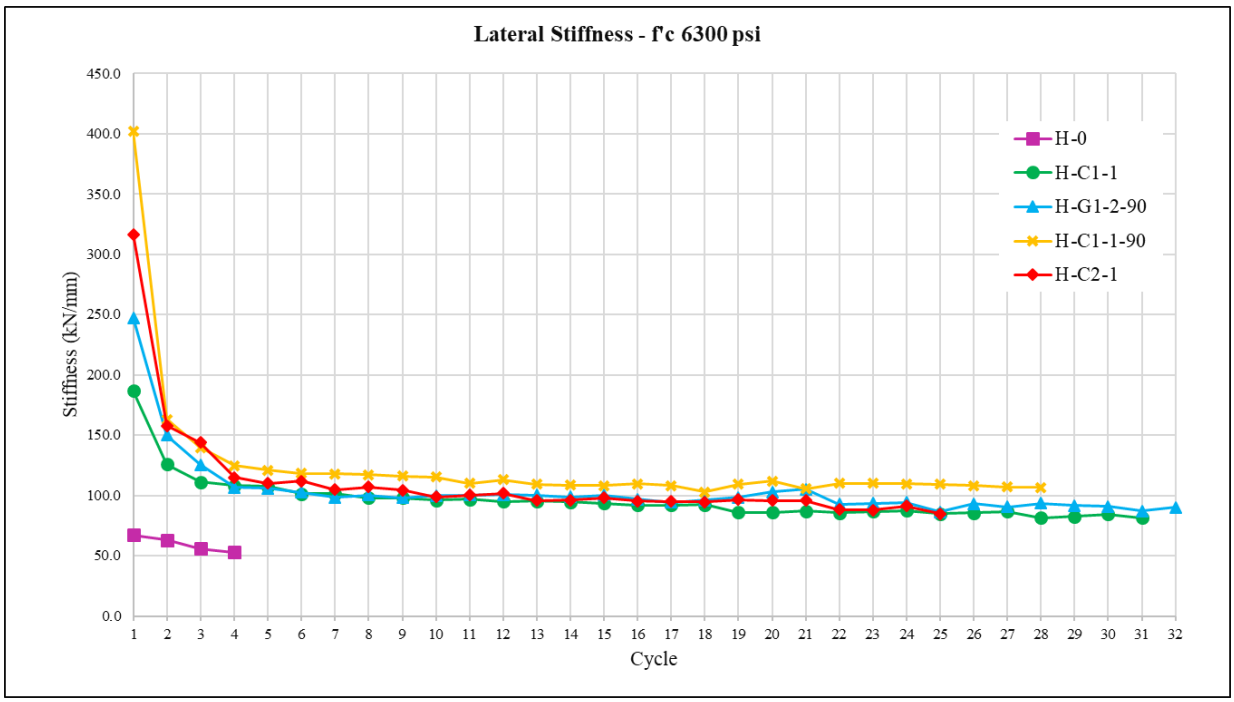

Figure 4.17 – Stiffness degradation, high strength specimens (f'c 6300 psi).

Own source

For the unreinforced specimen in the high strength specimens, the initial secant stiffness was 67 kN/mm, decreasing in 21% until 53 kN/mm up to failure. H-C1-1-90 had an initial secant stiffness of 402 kN/mm, compared to H-C1-1 that had 187 kN/mm, which evidence the advantage in deformation of wrapping the FRP around the corner. The specimens had a drop in stiffness of 73% and 56% for H-C1-1-90 and H-C1-1 respectively. H-C2-1 began with a secant stiffness of 317 kN/mm decreasing to 85 kN/mm, it represents a drop of 73%, Finally H-G1-2-90 had a good behavior considering was reinforced with GFRP, beginning with 247 kN/mm and decreasing to 90 kN/mm, a drop of 64%.

4.6 Energy dissipation capacity

"Energy dissipation is a basic structural property of RC elements when subjected to seismic demands" (Shen et al., 2017), the area within the hysteretic loops can be used as a measure of the energy dissipation capacities (Antoniades et al., 2007). Figure 4.18 and Figure 4.19 show the cumulative dissipated energy (kN.m) for each cycle for low and high strength specimens respectively, the cumulative dissipated energy was defined as the sum of the area enclosed by the loops in each cycle (Layssi et al., 2012).

Figure 4.18 shows the cumulative dissipated energy for the low strength specimens. As expected, de dissipated energy increased with the increase of each cycle, the unreinforced specimen reached a cumulative dissipated energy of 9.5 kN.m (7.0 kip.ft). The one-sided reinforced specimens showed a similar behavior, L-G1-1 had a little drop in cycles 13 to 17, the final cumulative dissipated energy of specimens L-C1-1 and L-G1-1 was 35.2 (26) and 28.8 (21.2) kN.m (kip.ft) respectively. This was an increasing of 270% for L-C1-1 and 203% for L-G1-1, which means that in spite of do not present a ductile behavior the reinforcement is able to absorb and dissipate a great amount of energy. For the two-sided reinforced specimens, the final values were 22.9 (16.9) and 21.8 (16.1) kN.m (kip.ft) for L-C1-2 and L-G1-2 respectively, both specimens after force control protocol (cycle 18) showed a drop in dissipate energy. The final values represented an increase of 140% and 129% respect of the unreinforced specimen, it was an expected behavior due to the reinforcement configuration (more rigid).

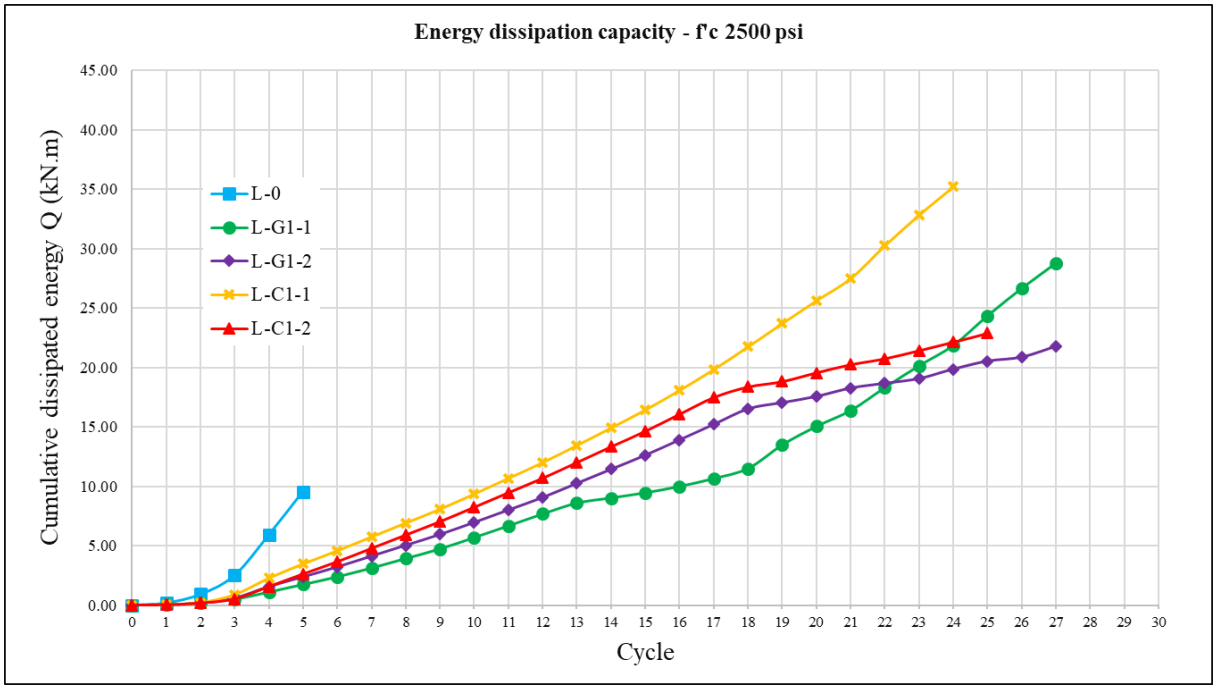

Figure 4.18 – Energy dissipation capacity (f'c 2500 psi).

Own source

Figure 4.19 shows the cumulative dissipated energy for the high strength specimens. As expected, the dissipated energy increased with the increase of each cycle, the unreinforced specimen reached a cumulative dissipated energy of 4.8 kN.m (3.5 kip.ft). All specimens had a similar behavior, some with more slope than others. The final cumulative dissipated energy was 29.8, 29.8, 27.6, and 37.1 kN.m for H-C1-1, H-C2-1, H-C1-1-90 and H-G1-2-90 respectively. The great contribution of FRP can be seen, allowing the walls absorb a great quantity of energy before failure. Representing an increasing of 521%, 521%, 475% and 674% respect the unreinforced specimen. H-C1-1 and H-C1-1-90 reached a similar final cumulative dissipated energy despite the deformation at failure was higher in H-C1-1.

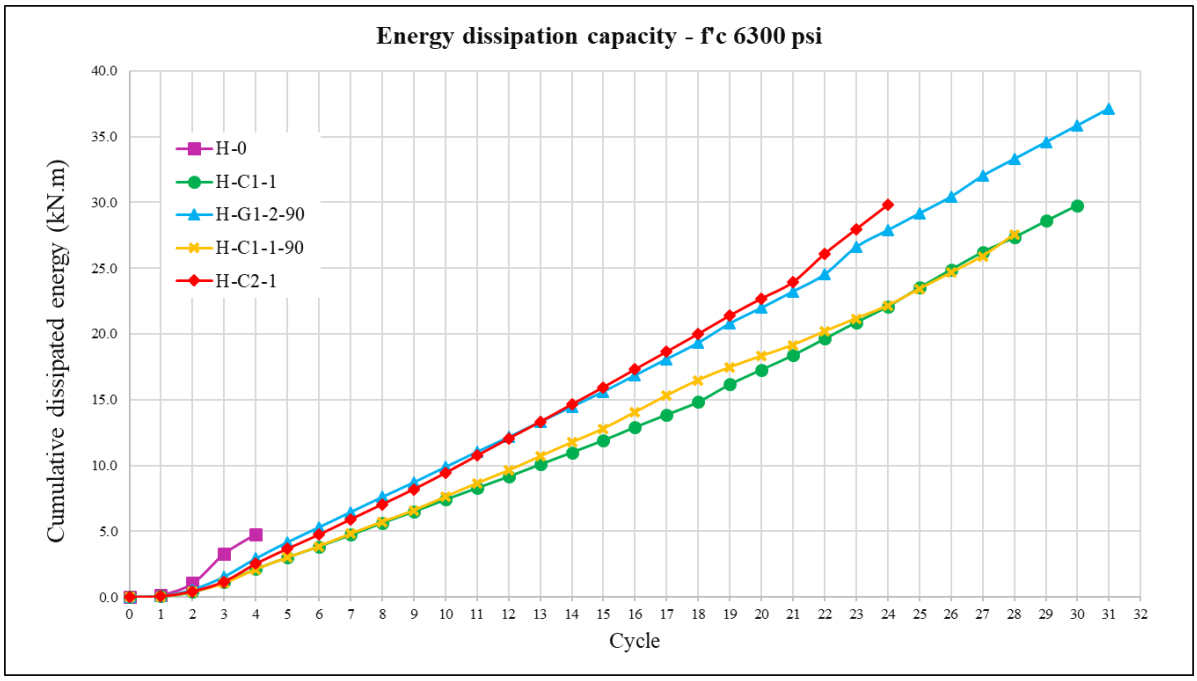

Figure 4.19 – Energy dissipation capacity (f'c 6300 psi).
Own source

4.7 Comparation with ACI 440.2

As previously mentioned, in accordance with the ACI 440.2R-17 the theoretical capacities were calculated. The equations used to compute the shear contribution of the FRP shear reinforcement were those given in chapter 11.4 for beams and columns, since they are the ones that take into account the possibility of placed fabrics FRP. However, the equations do not consider the possibility of one-sided reinforcement as do those given in chapter 13.7. Both equations consider bonded U-wraps and bonded face plies. Table 4.3 shows the equations given by the ACI 440.2R-17.

Table 4.3 – Base equations for calculating FRP shear contribution

11.4a equation (for a two-sided retrofit of beams and columns)	13.7.7.2.2c equation (for a two-sided retrofit of walls)	13.7.7.2.2c equation (for a one-sided retrofit of walls)
$V_f = \frac{A_{fv}\varepsilon_{fe}E_f(sin\alpha + cos\alpha)d_{fv}}{S_f}$	$V_f = 2t_f\varepsilon_{fe}E_f d_{fv}$	$V_f = 0.75t_f\varepsilon_{fe}E_f d_{fv}$

If only the horizontal FRP fabrics are considered, the equation given my chapter 11.4 can be transformed as follow:

11.4a equation (for a two-sided retrofit of beams and columns)	13.7.7.2.2c equation (for a two-sided retrofit of walls)	13.7.7.2.2c equation (for a one-sided retrofit of walls)
$V_f = \frac{2\varepsilon_{fe}nw_f t_f E_f d_{fv}}{S_f}$	$V_f = 2\varepsilon_{fe}t_f E_f d_{fv}$	$V_f = 0.75\varepsilon_{fe}t_f E_f d_{fv}$

The main variables that can affect the results are the number of sides reinforced and the effective strain in FRP reinforcement attained at failure. For the next comparison, only the 11.4a equation will be considered since it is the one that take into account the possibility of placed fabrics FRP. According to chapter 3.7, the effective strain in FRP reinforcement attained at failure can be calculated as follow:

$\varepsilon_{fe} = \kappa_v\varepsilon_{fu} \leq 0.004$

For practical effects, Figure 4.20 shows the experimental vs theoretical FRP shear capacity, in which the FRP shear contribution (experimental and theoretical) is divided by $\frac{2nw_f t_f E_f d_{fv}}{S_f}$ (one-sided reinforced specimens do not consider the 2) in order to evaluated the effective strain.

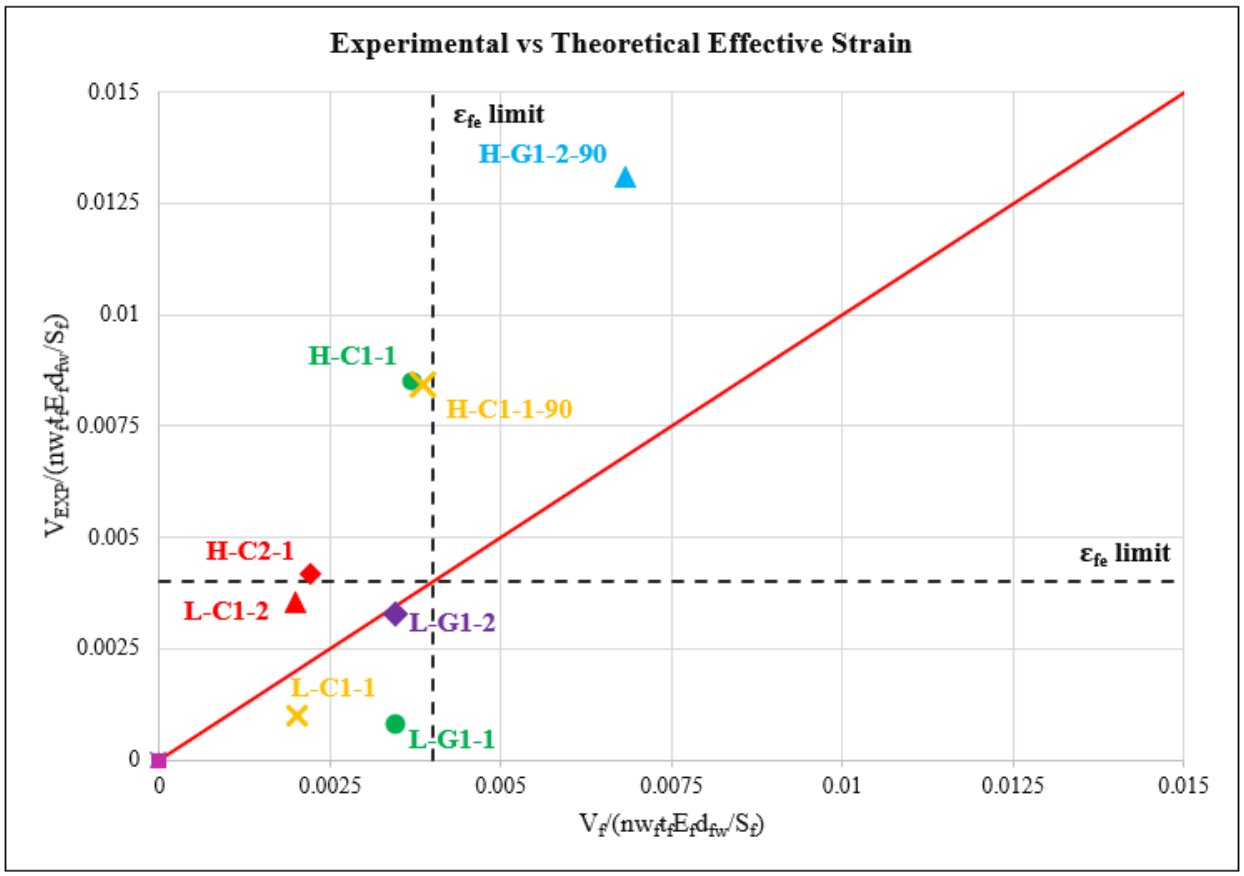

Figure 4.20 – experimental vs theoretical FRP effective strain.

Own source

When the theoretical capacity was calculated, the 0.004 limit (Triantafillou, 1998) was not taking into account; the figure shows that all specimens except by H-G1-2-90 were under this limit. On the other hand, all high strength specimens were experimentally above the limit. The low strength specimens were under the limit, but they were far from the theoretical except by L-G1-2.

The bond-reduction coefficient (κ_v) can be computed from eq. 11.

$$\kappa_v = \frac{k_1 k_2 L_e}{11900\varepsilon_{fu}} < 0.75 \quad (SI) \tag{16}$$

Where k_1 depends on the concrete strength and k_2 the reinforcement configuration:

$$L_e = \frac{23300}{(nt_f E_f)^{0.58}} \ (SI) \tag{17}$$

$$k_1 = \left(\frac{f'_c}{27}\right)^{2/3} \ (SI) \tag{18}$$

$$k_2 = \frac{d_w - 2L_e}{d_w} \ (for\ two\ sides\ bonded)$$
$$k_2 = \frac{d_w - L_e}{d_w} \ (for\ U-wraps) \tag{19}$$

If another graphic is made but now considering the design rupture strain of FRP reinforcement (ε_{fu}) the bond-reduction coefficient can be analyzed:

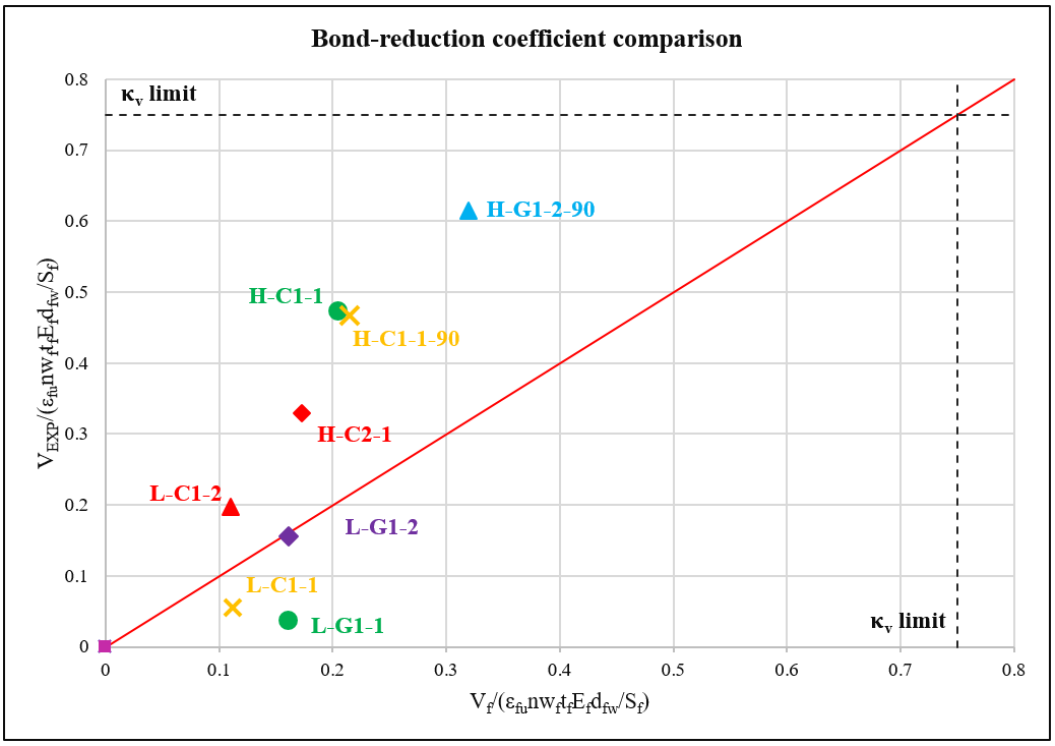

Figure 4.21 – Bond-reduction coefficient comparison.

Own source

The Figure 4.21 shows that for the high strength specimens the bond-reduction coefficient could be very low, about half of the experimental values. Since this coefficient

depends on the active bond length, the modification factors that account for the concrete strength and for the type of wrapping scheme is difficult carry out a specific analysis with the obtain data. To analyze each variable, the others are left as constants. First, the modification factor that account the concrete strength is analyzed, Figure 4.22 shows that contrary to what is theoretically expected, the greater the concrete strength, the better bond adherence. With the obtain data, an equation for k_1 can be established, $k_1 = ({f'c}/{26})^2$.

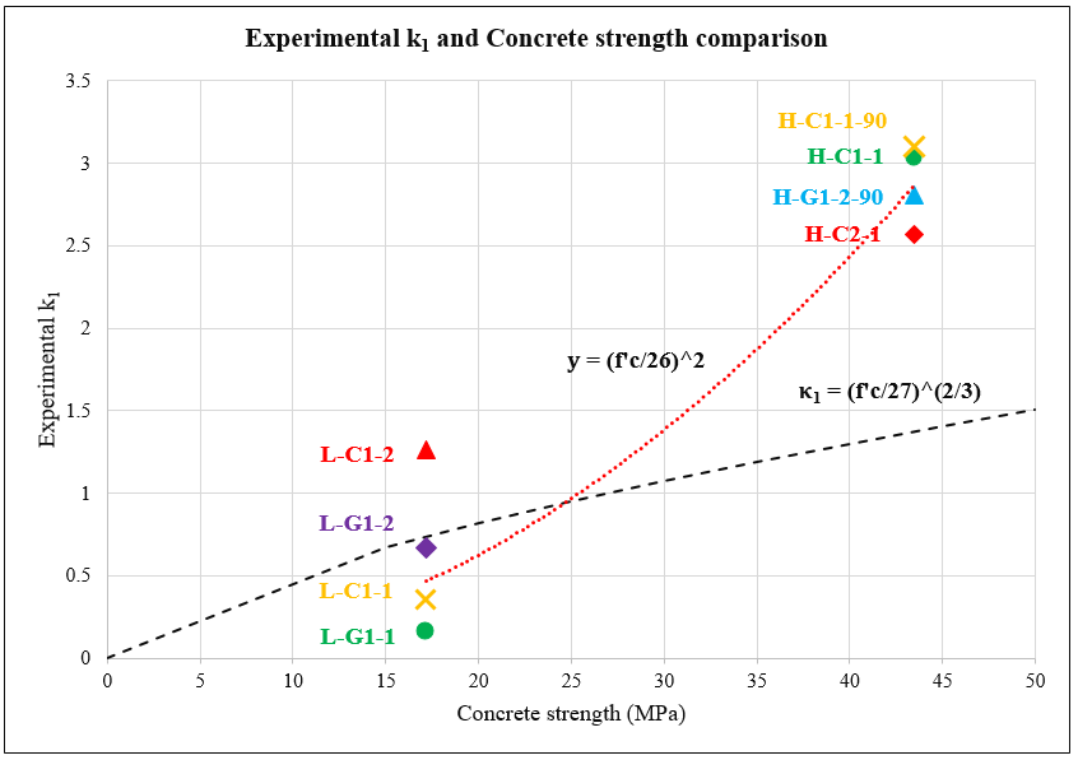

Figure 4.22 – Experimental k_1 and concrete strength comparison.
Own source

The Figure 4.23 shows the comparison between experimental k2 and FRP configuration, A lot of variability can be seen, therefore, carry out an analysis under this situation won't be representative. However, in the one-sided bonded reinforcement, it is clear the effect of the concrete strength (remember that k_1 was set as constant).

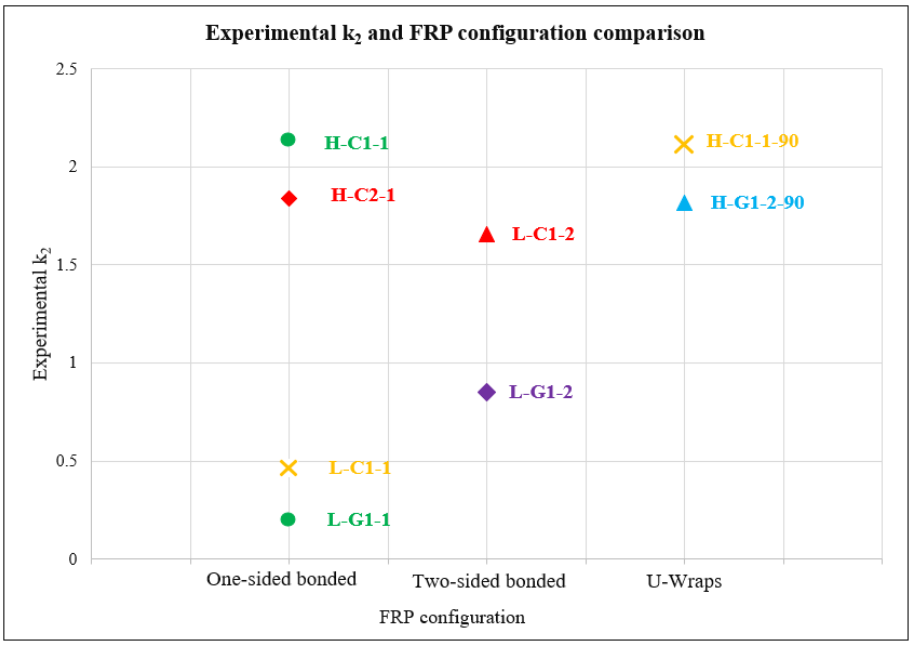

Figure 4.23 – Experimental k_2 and FRP configuration comparison.

Own source

As mentioned, the recommended additional reduction factor for FRP shear reinforcement (ψ_f) was not considered because the nominal shear strength was sought and only considers completely wrapped members and three-side or two-opposite-sides schemes. However, for practical purposes Figure 4.24 shows the theoretical shear strength considering the FRP reduction factor and the strength reduction factor for shear strength. For the low concrete compression strength specimens, the experimental values are closer to the theoretical. Figure 4.25 shows the experimental reduction factor, where the experimental FRP contribution is divided between the theoretical FRP contribution. It can be seen that for the high concrete compression strength the reduction factor is higher than 1.5, this was already analyzed with the k_1 factor. All experimental reduction factors were higher than 0.85 except for the low concrete strength reinforced by one-side.

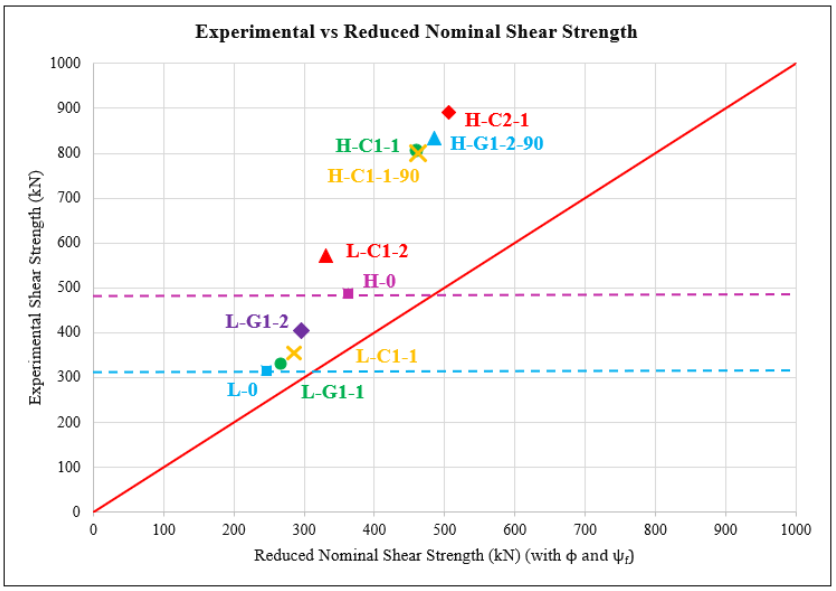

Figure 4.24 – Experimental vs Reduced Nominal Shear Strength (considering ϕ and ψ_f).

Own source

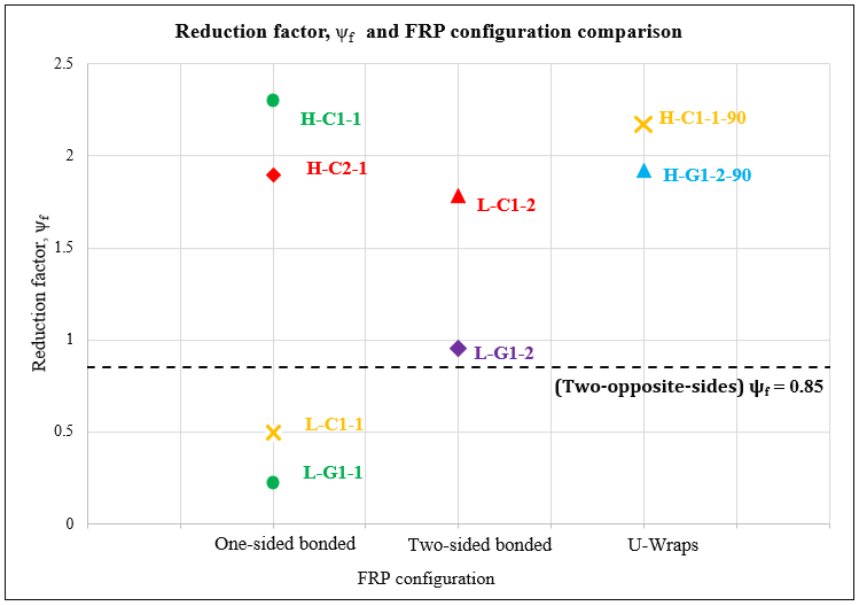

Figure 4.25 – Reduction factor ψ_f and FRP configuration comparison.

Own source

5. Conclusions and Recommendations

5.1 Conclusions

From the results obtained in the investigation project, the following conclusions are presented:

- The shear strength of a RC wall calculated by ACI 318-19 can be very conservative. For experimental purposes, to calculate the shear strength of a RC wall is recommendable to multiply the result by 1.43 as mentioned in (Sánchez-Alejandre & Alcocer, 2010).
- The horizontal FRP fabrics externally bonded with the purpose of enhancement the shear capacity of a RC wall showed great performance, increasing the capacity in ranges from 3% to 78%. These increases of shear strength were also related to changes in the deformation behavior, which presented changes in ranges from -26% to 83% with respect to the unreinforced specimen.
- Regarding to the low strength specimens, the ones reinforced with CFRP showed the best performance increasing the shear capacity by 11% in the one-sided reinforcement specimen and 79% in the two-sided reinforcement specimen. Meaning a 23% and 61% with respect to the specimens reinforced with GFRP fabrics, respectively.
- The high strength specimens made the biggest gains, showing a minimum increase in shear strength of 61% in the H-C1-1 specimen, this can be related to a better bond because of the high concrete strength. The H-C2-1 specimen gained the most with an increase of 83%.

- The results showed experimental capacities lower than theoretical expected for one-sided reinforced low strength specimens. This capacity was calculated according to ACI 440.2R-17 equations given for beams and columns reinforcement. The equations give in chapter 13.7 for walls reinforcement specify a reduction of 25% when reinforcement in one-sided, according to the previous results, this reduction could be 10%. For two-sided reinforced low strength specimens, the results showed shear strengths higher than expected with some variability that could be related with other factors.
- Wrapping the FRP fabric around the corner does not increase the shear capacity but affects the deformation capacity. H-C1-1 reached 36% higher deformation at failure compared with H-C1-1-90 which was wrapped around the corner.
- The low strength specimens reinforced with CFRP showed higher shear strengths but lower deformations at failure compared with the specimens reinforced with GFRP. However, the CFRP specimens were able to dissipate more energy up to failure.
- The expected failure was shear failure because of the TRCW design, this is a brittle and sudden failure, therefore, the wall initial stiffness could change depending on the reinforcement configuration and do not present the same behavior as flexural reinforcement where the initial stiffness both in the unreinforced and reinforced specimens is the same.
- The low strength specimens presented an average decrease in stiffness of 67%, the unreinforced specimen stiffness degradation was 32%, meaning in a degradation of more than double before failure. The high strength specimens also showed an average decrease in stiffness of 67% compared with the 21% of the unreinforced specimen.
- According to the energy dissipation capacity, the specimens showed similar behaviors. For the low strength specimens, L-C1-1 was the one that dissipated the most with a cumulative

dissipated energy of 35.2 kN.m compared with the 9.5 kN.m of the unreinforced specimen. Despite the fact that the GFRP specimens reached a higher deformation, the CFRP ones reached higher cumulative dissipated energy. For the high strength specimens, H-G1-2-90 reached 37.1 kN.m of cumulative dissipated energy compared with the 4.8 kN.m of the unreinforced specimen, showing that wrapping around the corners only affects the deformation capacities but no the dissipated energy.

- The effective strain in FRP reinforcement attained at failure could be higher in high concrete strength walls due to their good bond capacity. The modification factor that takes into account the concrete strength in the ACI 440.2R-17 could be modified for $k_1 = (f'c/26)^2$ when is used in wall reinforcement.
- The recommended additional reduction factor for FRP shear reinforcement does not take into account the possibility of different schemes in walls. However, due to the lack of enough tests and the variability in other parameters it is difficult to stablishes a value for the different schemes.

5.2 Recommendations

Below are a series of recommendations that could be made in the future in order to deepen and strengthen some aspects of this investigation or when undertaking similar investigations.

1. It is recommended to continue carrying out tests on RC walls reinforced with FRP fabrics to be able to calibrate the different factors that intervene in the calculation of the contribution to the shear capacity provided by the FRP.

2. It is recommended to experimentally evaluate RC walls with similar characteristics, considering other FRP reinforcement schemes and verify their contribution to shear capacity.

3. It is recommended to carry out tests taking into account the impact of the axial load on the contribution to the shear capacity.

A. Annex: Hysteresis Curves

Annex A: Hysteresis Curves, shows the remaining curves for TRCW specimens

Applied load versus mid-span displacement cycles for L-0 specimen

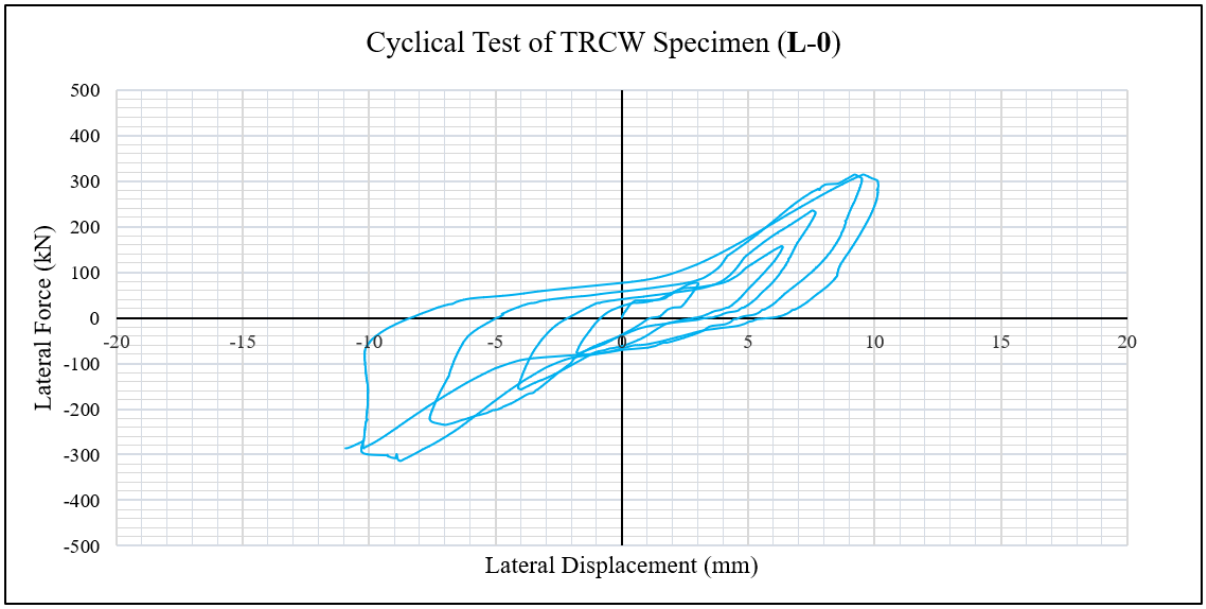

Applied load versus mid-span displacement cycles for L-G1-2 specimen

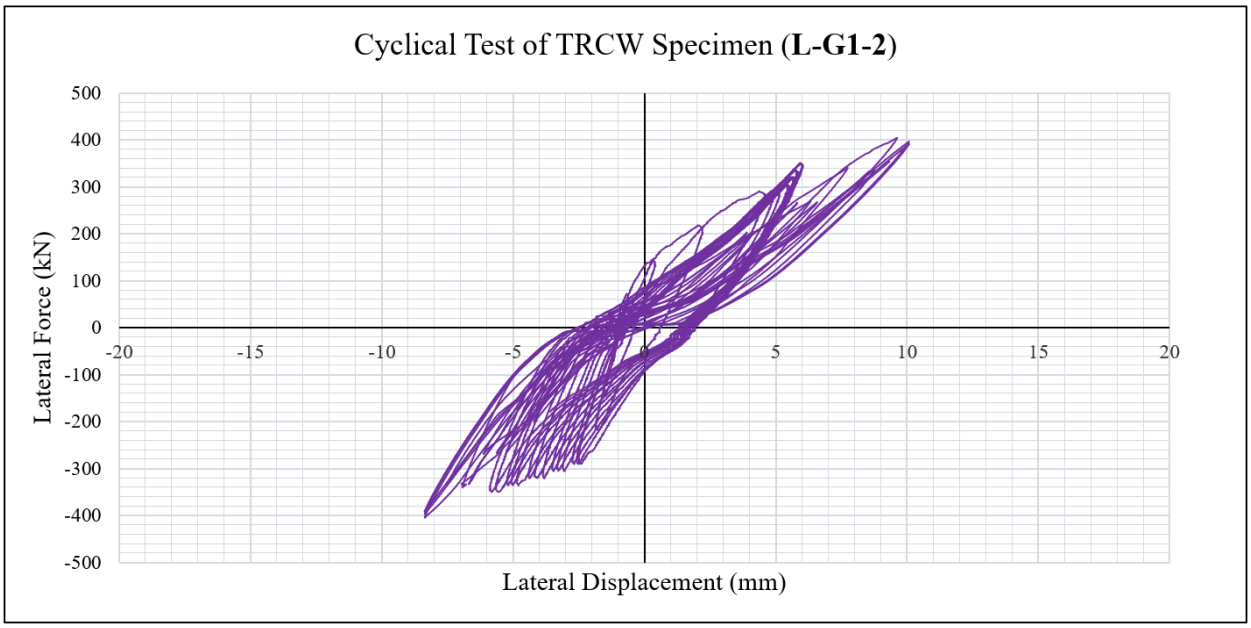

Applied load versus mid-span displacement cycles for L-C1-1 specimen

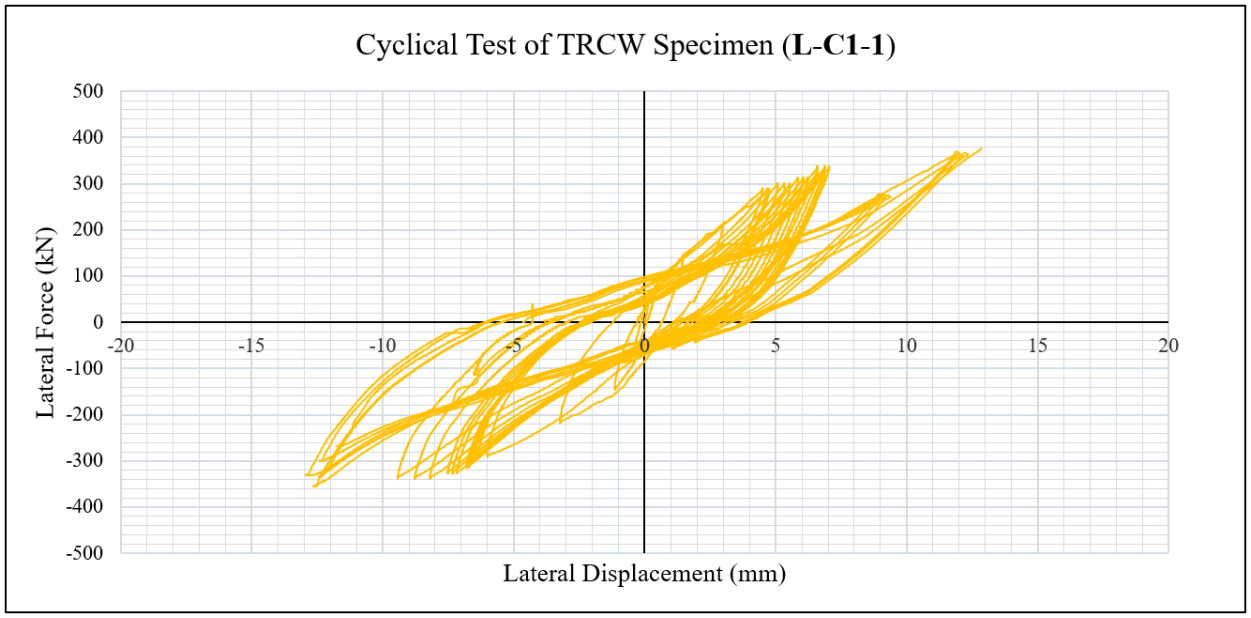

Applied load versus mid-span displacement cycles for L-C1-2 specimen

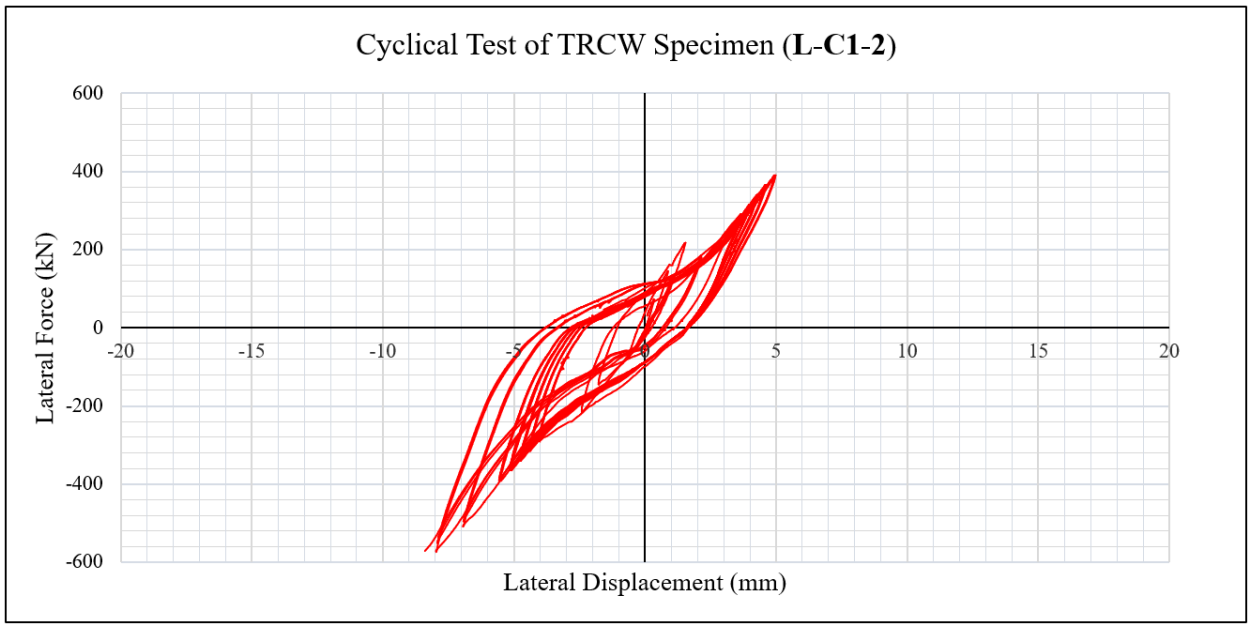

Applied load versus mid-span displacement cycles for H-0 specimen

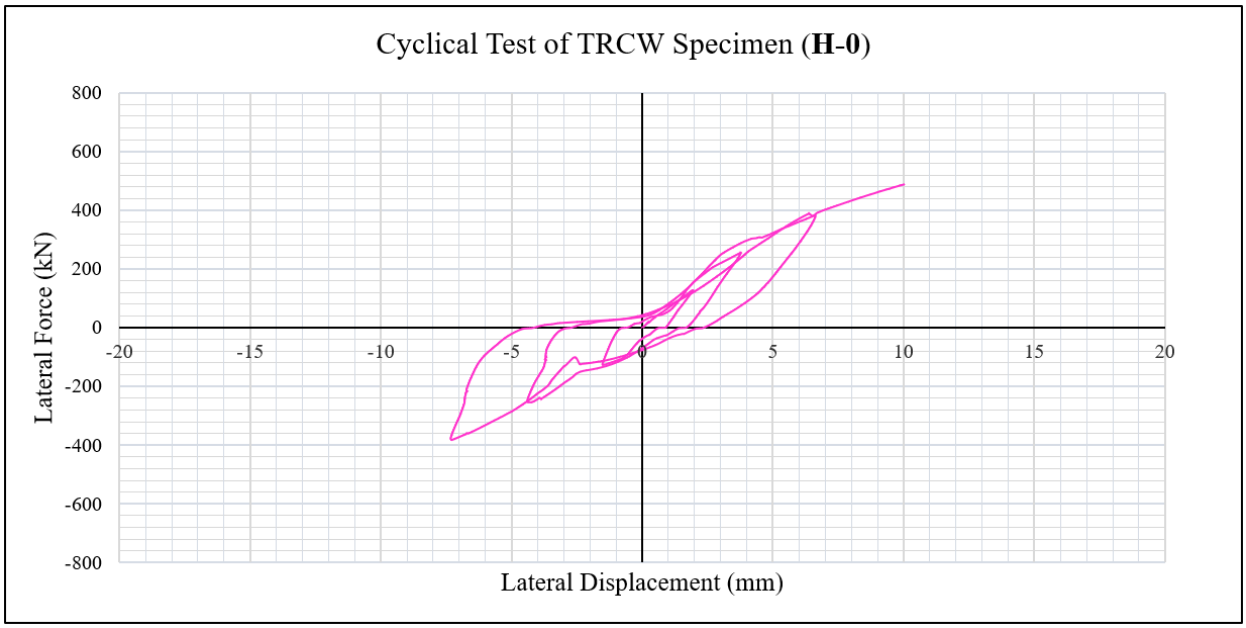

Applied load versus mid-span displacement cycles for H-C1-1 specimen

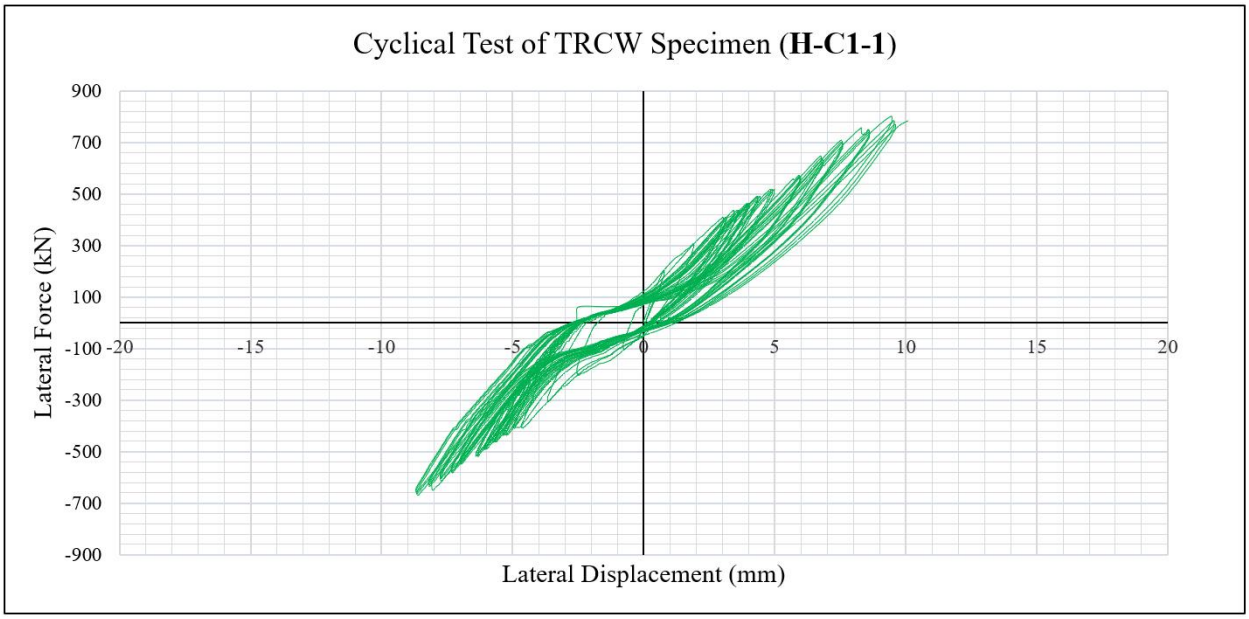

Applied load versus mid-span displacement cycles for H-C21 specimen

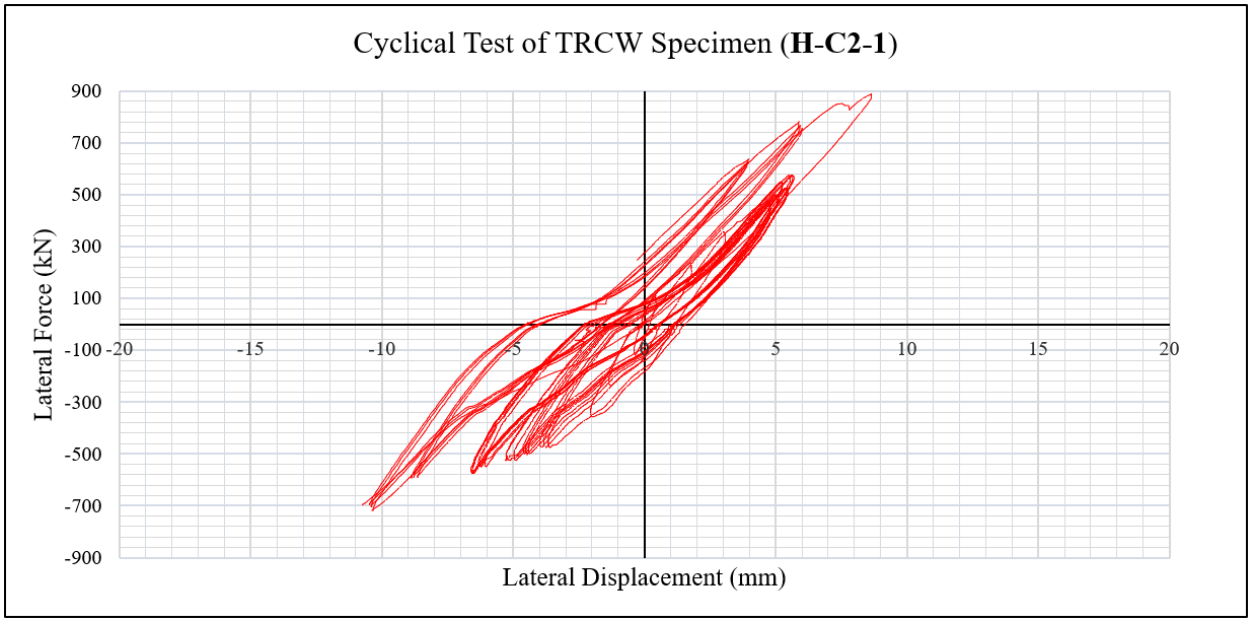

Applied load versus mid-span displacement cycles for H-G1-2-90 specimen

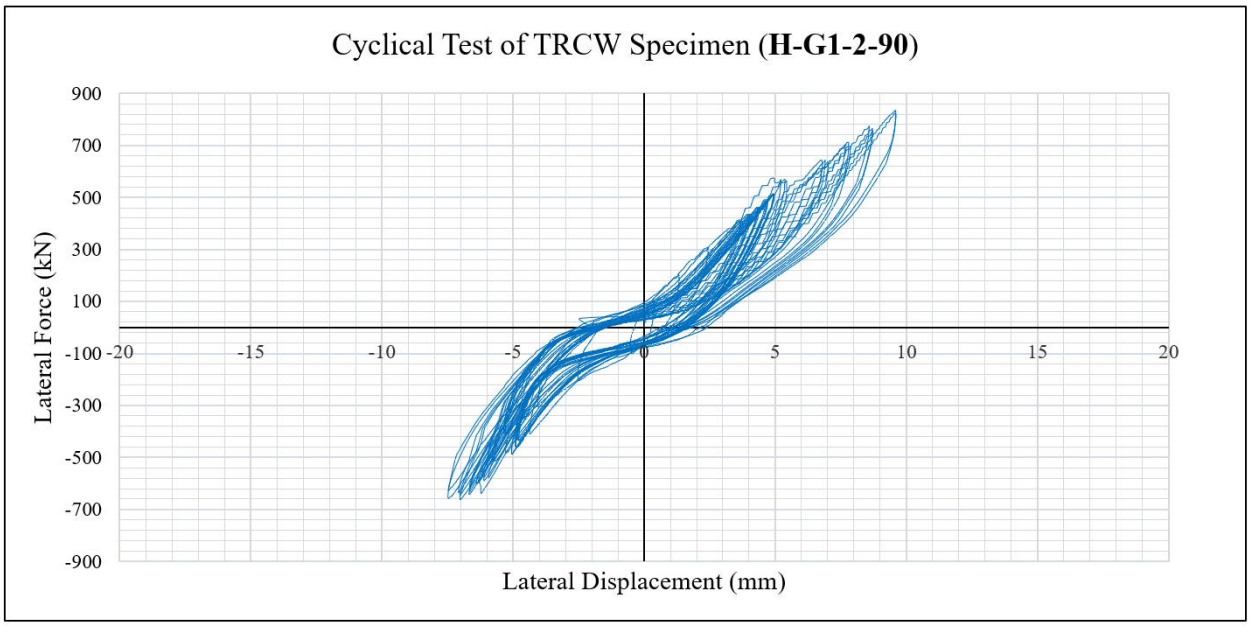

Applied load versus mid-span displacement cycles for H-C1-2-90 specimen

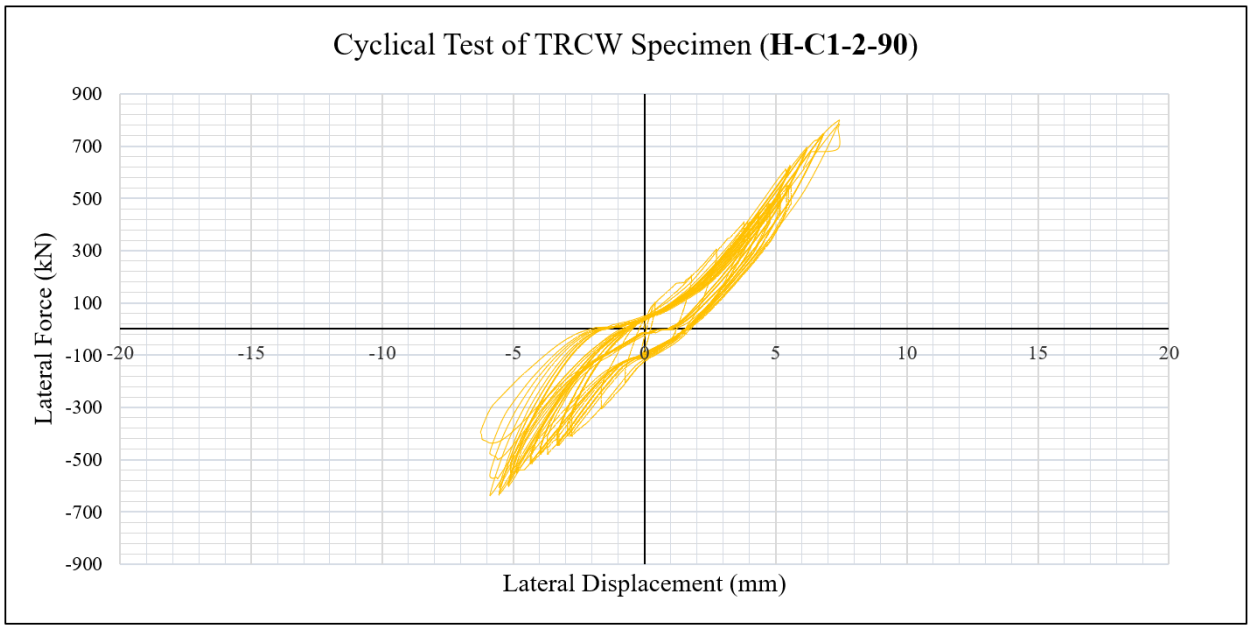

B. Annex: FRP reinforcement design

Annex B: FRP reinforcement design, contains the FRP reinforcement design of L-G1-1 specimen. Table 3.9 and Table 3.3 contain the design's input data.

Property		Value	
Wall height	h_w	2.6 m	102.4 in
Wall length	l_w	1.3 m	51.2 in
Wall thickness	t_w	0.1 m	3.9 in
Low concrete strength	f'_c	17.2 MPa	2500 psi
Shear strength of the wall for low f'c	V_R	320 kN	71.9 kip
Effective depth of the shear wall	d_w	1.215 m	47.8 in
Nominal thickness of one ply of FRP reinforcement	t_f	1.02 mm	0.04 in
Design rupture strain of FRP reinforcement	ε_{fu}	0.0213	0.0213
Modulus of elasticity	E_f	26683 MPa	$3.87*10^6$ psi
Width of FRP reinforcing plies	w_f	0.076 m	3.0 in
Center-to-center spacing of FRP	S_f	360 mm	14.17 in

The shear strength provided by the FRP is calculated using:

$$V_f = \frac{A_{fv} f_{fe} (sin\alpha + cos\alpha) d_{fv}}{S_f}$$

The area of FRP external reinforcement is calculating as follow:

$$A_{fv} = n t_f w_f = 1 \cdot 1.02 \cdot 76 = 77.2\ mm^2$$

The effective strain in FRP reinforced attained at failure (ε_{fe}) is calculated according to chapter 11.4.1 of the guide:

$$\varepsilon_{fe} = \kappa_v \varepsilon_{fu} \leq 0.004$$

The bond-reduction coefficient (κ_v) can be computed from equation:

$$\kappa_v = \frac{k_1 k_2 L_e}{11900\varepsilon_{fu}} < 0.75$$

Where:

$$L_e = \frac{23300}{(nt_f E_f)^{0.58}} = \frac{23300}{(1 * 1.02 * 26683)^{0.58}} = \mathbf{62.54\ mm}$$

$$k_1 = \left(\frac{f'_c}{27}\right)^{2/3} = \left(\frac{17.2}{27}\right)^{2/3} = \mathbf{0.740}$$

$$k_2 = \frac{d_w - 2L_e}{d_w} = \frac{1.112 - 2(0.06254)}{1.112} = \mathbf{0.888}$$

The bond-reduction coefficient (κ_v) is calculated as follow:

$$\kappa_v = \frac{0.74 * 0.888 * 62.54}{11900 * 0.0213} = \mathbf{0.1621}$$

With the bond-reduction coefficient calculated, the effective strain in FRP reinforcement attained at failure can be calculated (for high concrete strength specimens, 0.004 limit wasn't considered)

$$\varepsilon_{fe} = \kappa_v \varepsilon_{fu} = 0.1621 * 0.0213 = \mathbf{0.00345}$$

The shear strength provided by FRP:

$$V_f = \frac{A_{fv}\varepsilon_{fe}E_f(sin\alpha + cos\alpha)d_{fv}}{S_f} = \frac{77.2 \cdot 0.00345 \cdot 26683 \cdot 1112}{360} = \mathbf{22\ kN}$$

Finally, as the L-C1-1 specimen would be subjected to double shear strength, the shear strength value calculated provided by the FRP had to be multiplied by 2.

$$P_{n,FRP} = \mathbf{44\ kN}$$

C. Annex: Stress-Strain Curve for Steel

Annex C: Stress-Strain curve for steel shows the tensile testing on steel rod number 4 using during specimen's construction.

Nominal diameter	½ in
Length	25 cm
Load (kg)	Def (10^{-2} mm)
0	0.0
500	3.0
1000	7.0
1500	11.0
2000	16.0
2500	21.0
3000	26.0
3500	31.0
4000	36.0
4500	41.0
5000	46.0
5656	55.0
5872	65.0
5850	75.0
5830	88.0
5848	100.0
Yield load	**5830**
Maximum load	**8026**
Elongation	**23.3 cm**

The stress-strain curve is graphed, and according to NTC 2289 (ASTM A706/A706M), the yield stress is 450 MPa (see blue line).

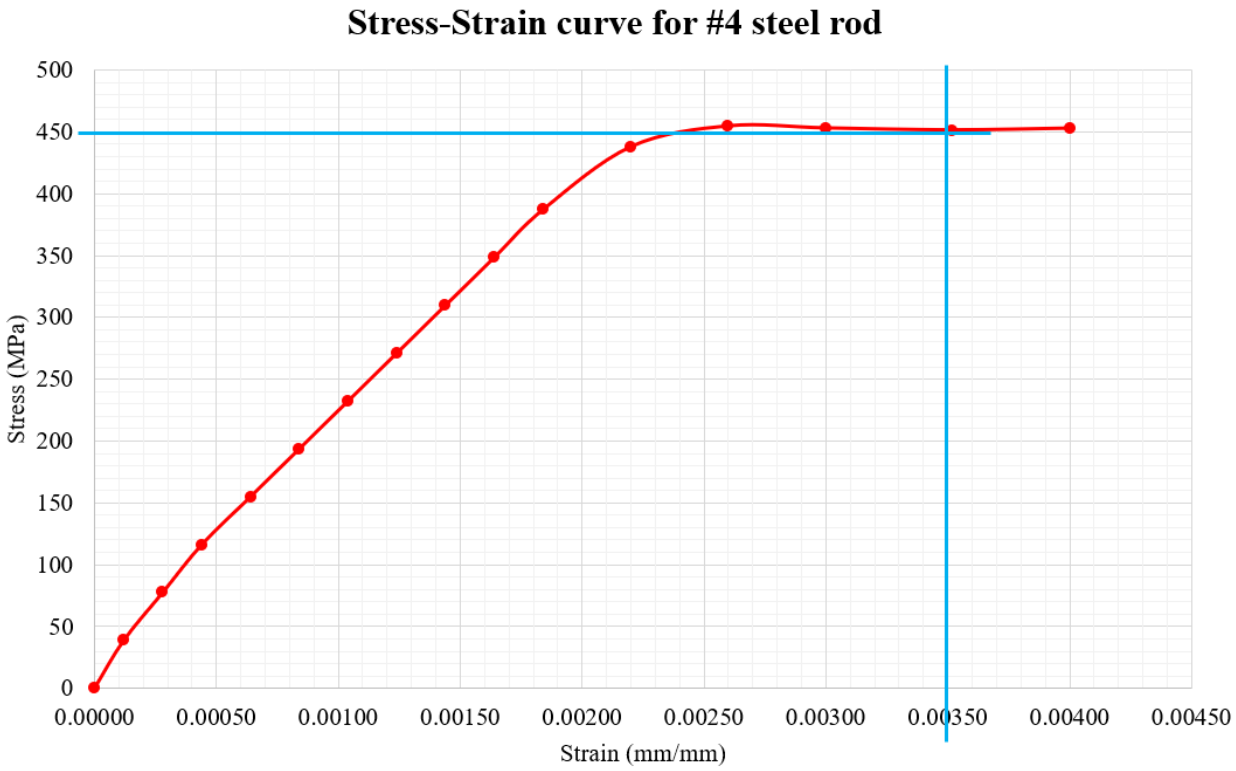

Bibliography

Altin, S., Anil, Ö., Kopraman, Y., & Kara, M. E. (2013). Hysteretic behavior of RC shear walls strengthened with CFRP strips. *Composites Part B: Engineering*, *44*(1), 321–329. https://doi.org/10.1016/j.compositesb.2012.05.009

American Concrete Institute (ACI) Committee 318. Building Code Requirements for Structural Concrete and Commentary (Farmington). (2019).

American Concrete Institute (ACI) Committee 440. 440.2R-17: Guide for the Design and Construction of Externally Bonded FRP Systems for Strengthening Concrete Structures. (2017).

Antoniades, K. K., Salonikios, T. N., & Kappos, A. J. (2007). Evaluation of hysteretic response and strength of repaired R/C walls strengthened with FRPs. *Engineering Structures*, *29*(9), 2158–2171. https://doi.org/10.1016/j.engstruct.2006.11.021

Ávila, O., Carrillo, J., & Alcocer, S. M. (2011). Rehabilitación de muros de concreto usando CRFA: ensayos en mesa vibradora. *Concreto y Cemento: Investigación y Desarrollo*, *2*(2), 2–17.

Belarbi, A., & Acun, B. (2013). *FRP Systems in Shear Strengthening of Reinforced Concrete*

Structures. *57*, 2–8. https://doi.org/10.1016/j.proeng.2013.04.004

Blandón, C. A., Rave-Arango, J. F., & Bonett-Díaz, R. L. (2015, May). Behavior of thin reinforced concrete walls under lateral load. *VII Congreso Nacional de Ingeniería Sísmica*.

Borri, A., Castori, G., & Corradi, M. (2015). Determination of Shear Strength of Masonry Panels Through Different Tests. *International Journal of Architectural Heritage*, *9*(8), 913–927. https://doi.org/10.1080/15583058.2013.804607

Carrillo, J., & Alcocer, S. M. (2012). Acceptance Limits for Performance-Based Seismic Design of RC Walls for Low-Rise Housing. *Earthquake Engineering & Structural Dynamics*, *41*(15). https://doi.org/10.1002/eqe.2186

Carrillo, J., & Alcocer, S. M. (2013). Shear Strength of Reinforced Concrete Walls for Seismic Design of Low-Rise Housing. *Earthquake Spectra*, *110*(3). https://doi.org/10.14359/51685599

CEER (Colombian Earthquake Engineering Research Network). (2018). *Estudio del Comportamiento Sísmico de Edificios de Muros Delgados de Concreto Reforzado* (Issue 002). https://doi.org/10.13140/RG.2.2.17919.97445

Christidis, K. I., Vougioukas, E., & Trezos, K. G. (2016). Strengthening of non-conforming RC shear walls using different steel configurations. *Engineering Structures*, *124*, 258–268. https://doi.org/10.1016/j.engstruct.2016.05.049

Cruz-Noguez, C. A., Lau, D. T., Sherwood, E. G., Hiotakis, S., Lombard, J., Foo, S., & Cheung, M. (2015). Seismic Behavior of RC Shear Walls Strengthened for In-Plane Bending Using Externally Bonded FRP Sheets. *Journal of Composites for Construction*, *19*(1), 04014023. https://doi.org/10.1061/(asce)cc.1943-5614.0000478

Dan, D. (2012). Experimental tests on seismically damaged composite steel concrete walls retrofitted with CFRP composites. *Engineering Structures*, *45*, 338–348. https://doi.org/10.1016/j.engstruct.2012.06.037

El-Sokkary, H., & Galal, K. (2013). Seismic Behavior of RC Shear Walls Strengthened with Fiber-Reinforced Polymer. *Journal of Composites for Construction*, *17*(5), 603–613. https://doi.org/10.1061/(asce)cc.1943-5614.0000364

Fintel, M. (1995). Performance of buildings with shear walls in earthquakes of the last thirty years. *PCI Journal*, *40*(3), 62–80. https://doi.org/10.15554/pcij.05011995.62.80

Haroun, M. A., Mosallam, A. S., & Allam, K. H. (2005). Cyclic In-Plane Shear of Concrete Masonry Walls Strengthened by FRP Laminates. *Fiber-Reinforced Polymer (FRP) Reinforcement for Concrete Structures : [Proceedings of the Seventh International Symposium of the Fiber-Reinforced Polymer Reinforcement for Reinforced Concrete Structures (FRPRCS-7), Kansas City, Missouri, November 6-9*, *20*, 327–340.

Huang, Z., Shen, J., Lin, H., Song, X., & Yao, Y. (2020). Shear behavior of concrete shear walls with CFRP grids under lateral cyclic loading. *Engineering Structures*, *211*(March). https://doi.org/10.1016/j.engstruct.2020.110422

ICRI Guideline No. 310.2R-2013: Selecting and Specifying Concrete Surface Preparation for Sealers, Coatings, Polymer Overlays, and Concrete Repair. (2013). *310*.

Jiang, L., Li, H., Liu, L., & Zhang, J. (2014). *Research Summary of Strengthening RC Shear Walls*. *504*, 969–976. https://doi.org/10.4028/www.scientific.net/AMM.501-504.969

Khomwan, N., Foster, S. J., & Campus, K. (2005). *Fe modelling of frp-strengthened rc shear walls subjected to reverse cyclic loading*. *Bbfs*, 519–524.

Layssi, H., Cook, W. D., & Mitchell, D. (2012). Seismic Response and CFRP Retrofit of Poorly Detailed Shear Walls. *Journal of Composites for Construction*, *16*(3), 332–339. https://doi.org/10.1061/(asce)cc.1943-5614.0000259

Lombard, J., Lau, D., & Humar, J. (2000). Seismic strengthening and repair of reinforced concrete shear walls. *Proc., 12th World Conf. on …*, 1–8. http://www.iitk.ac.in/nicee/wcee/article/2032.pdf

Reglamento Colombiano de Construcción Sismo Resistente NSR-10. (2012). Asosiación Colombiana de Ingeniería Sísmica (AIS).

Rosso, A., Almeida, J. P., & Beyer, K. (2016). Stability of thin reinforced concrete walls under cyclic loads: state-of-the-art and new experimental findings. *Bulletin of Earthquake Engineering*, *14*(2), 455–484. https://doi.org/10.1007/s10518-015-9827-x

Samad, A. A. A., Mohamad, N., Ali, N., Jayaprakash, J., & Mendis, P. (2016). Rehabilitation of continuous reinforced concrete beams in shear by external bonding of carbon fiber reinforced polymer strips for sustainable construction. *Key Engineering Materials*, *708*(August), 49–58. https://doi.org/10.4028/www.scientific.net/KEM.708.49

San Bartolomé, Á. (2010). *Terremoto de Chile 27-02-2010*.

San Bartolomé, A., Muñoz, A., Villagarcía, M., & Acuña, C. (2007). *Comportamiento Sísmico De Placas De Concreto Reforzadas Con Mallas Electrosoldadas*.

Sánchez-Alejandre, A., & Alcocer, S. M. (2010). Shear strength of squat reinforced concrete walls subjected to earthquake loading — trends and models. *Engineering Structures*, *32*(8), 2466–2476. https://doi.org/10.1016/j.engstruct.2010.04.022

Shen, D., Yang, Q., Jiao, Y., Cui, Z., & Zhang, J. (2017). Experimental investigations on

reinforced concrete shear walls strengthened with basalt fiber-reinforced polymers under cyclic load. *Construction and Building Materials*, *136*(April), 217–229. https://doi.org/10.1016/j.conbuildmat.2016.12.102

Triantafillou, T. C. (1998). Shear strengthening of reinforced concrete beams using epoxy-bonded FRP composites. *ACI Structural Journal*, *95*(2), 107–115. https://doi.org/10.14359/531

Zhou, Y. W., Wu, Y. F., Teng, J. G., & Leung, A. Y. T. (2009). Ductility analysis of compression-yielding FRP-reinforced composite beams. *Cement and Concrete Composites*, *31*(9), 682–691. https://doi.org/10.1016/j.cemconcomp.2009.06.007